NASA TECHNICAL NOTE

NASA TN D-1980

SHOCK ENVELOPES OF BLUNT BODIES AT LARGE ANGLES OF ATTACK

by George E. Kaattari

Ames Research Center
Moffett Field, California

NATIONAL AERONAUTICS AND SPACE ADMINISTRATION • WASHINGTON, D. C. • DECEMBER 1963

SHOCK ENVELOPES OF BLUNT BODIES AT LARGE ANGLES OF ATTACK

By George E. Kaattari

Ames Research Center
Moffett Field, Calif.

NATIONAL AERONAUTICS AND SPACE ADMINISTRATION

For sale by the Office of Technical Services, Department of Commerce,
Washington, D.C. 20230 -- Price $1.25

ERRATA

NASA Technical Note D-1980

SHOCK ENVELOPES OF BLUNT BODIES AT LARGE ANGLES OF ATTACK

By George E. Kaattari
December 1963

Completed 25 Feb 64 fa

Page 5: The right-hand portion of equation (2) should be replaced by

$$c_1\left(\frac{r}{r_{max}}\right) + c_3\left(\frac{r}{r_{max}}\right)^3$$

Page 8: The term, $\tan\left(\sin^{-1}\frac{d}{R_{bs}}\right)$, appearing in equation (5c) should be replaced by $\tan\left(\sin^{-1}\frac{d}{2R_{bs}}\right)$.

Page 33: The symbols denoting measured values in the key of figure 8 should be half-solid for $M = 4.06$ and solid for $M = 5.45$.

SHOCK ENVELOPES OF BLUNT BODIES AT LARGE ANGLES OF ATTACK

By George E. Kaattari

SUMMARY

A method is presented for determining shock-wave shapes and stagnation-point locations for spherically blunted bodies at angle of attack. The method is applicable to perfect gas flows and equilibrium flow of real gases. The effects of altitude and velocity enter solely through the normal-shock density ratio appropriate to the flight conditions. The results given by the method are compared with experimental values and are shown to agree satisfactorily.

INTRODUCTION

Vehicles currently considered for atmosphere entry have blunt forward surfaces on which large aerodynamic forces and high heating rates develop. These forces and heating rates are related to the strength and orientation of the shock envelope over the forward portion of the vehicle.

A method for predicting shock envelopes ahead of spherically blunted bodies was presented in reference 1. A procedure, based on the predicted shocks of reference 1, was presented in reference 2 for estimating stagnation-point locations and the pressure, density, and temperature field in the shock layer ahead of spherically blunted bodies.

The purpose of this report is to present an improved method for determining the shock envelope and stagnation point. The method is applicable to a wider variation in body geometry and to a larger angle-of-attack range than that of references 1 and 2. It is based on an empirical correlation of the change in shock-layer thickness with angle of attack. This correlation was discovered through study of the experimental results of a systematic series of tests of a blunt body in the Mach number range 3.28 to 5.45. These experimental results as measured and in correlated form are presented herein.

NOTATION

b_1, b_n constants in stagnation-point function

c_1, c_3 constants in shock correlation function

d maximum diameter of body, ft

$d(\ )$ differential operator

M	free-stream Mach number
n	exponent in stagnation-point function
r	radial coordinate of shock or body measured from body axis of symmetry, ft
r_{max}	maximum radius of body, ft
r_{st}	radial distance to stagnation point on body, ft
r_t	radial location of tangent point of forebody and corner radius, ft
R_c	radius of body corner, ft
R_{cs}	shock radius near body corner (fig. 10), ft
R_b	forebody radius, ft
R_{bs}	basic shock radius at $\alpha = 0^\circ$, ft
x	coordinate of shock measured from plane normal to body axis at location Δ_o (fig. 3), ft
α	angle of attack, deg
α_{max}	maximum angle of attack for which shock correlation function is valid, deg
α_N	minimum angle of attack for which Newtonian theory gives valid stagnation-point location, deg
δ	stream direction behind inclined shock with respect to free-stream direction, deg
Δ	shock-layer thickness at location r in direction of body axis, ft
Δ_o	shock-layer thickness at body center line, ft
Δ^*	shock-layer thickness at sonic point when $\alpha = 0^\circ$, ft
ϵ	angle subtended by point on body at location r with respect to body axis $\epsilon = \sin^{-1}\frac{r}{R_b}$, deg
ϵ_a	afterbody surface inclination with respect to body axis (fig. 3), deg
ϵ_t	subtended angle of tangent point r_t with respect to body axis, $\epsilon_t = \sin^{-1}\frac{r_t}{R_b}$, deg
η	shock correlation function

θ_b^* inclination of sonic point on body with respect to plane normal to free-stream direction, deg

θ_s shock inclination at point r on shock with respect to plane normal to free-stream direction, $\alpha = 0^\circ$, deg

$\theta_{s\alpha}$ shock inclination at point r on shock with respect to plane normal to free-stream direction at angle of attack, deg

θ_s^* shock inclination opposite sonic point on body with respect to plane normal to free-stream direction, deg

Λ_c angle between line connecting two-dimensional shock center to sonic point on body with respect to free-stream direction (fig. 10), deg

Λ_s angle between line connecting most forward point of two-dimensional shock to sonic point on body with respect to free-stream direction (fig. 10), deg

$\frac{\rho_2}{\rho_1}$ density ratio across normal shock

Φ angular coordinate centered on vehicle axis of symmetry with respect to vertical plane, deg

TESTS AND PROCEDURE

Two models of a blunt-faced body, shown in figure 1, were tested in the Ames 1- by 3-foot wind tunnel at Mach numbers of 3.28, 4.06, and 5.45 at Reynolds numbers of 4.2×10^6, 3.5×10^6, and 2.7×10^6 per foot, respectively. The range of angles of attack was 0° to 60°. The low-angle model was supported by a sting coaxial with the model axis of symmetry. The high-angle model was supported by a sting attached to the lower portion of the model and inclined 45° to the model axis. The high-angle model was provided to minimize possible model support effects on the shock at angles of attack above 25°.

To establish shock-wave location, shadowgraphs of the body bow shock were taken in orthogonal planes at each of the three Mach numbers. Tests to determine the location of the stagnation point were made only at Mach number 3.28. The procedure for determining stagnation-point location was to wet the forward face of the model with a mixture of white lead and light oil and to allow the model to dry in the wind tunnel at the desired angle of attack. Photographs were taken of the stream patterns formed on the face of the model.

EXPERIMENTAL RESULTS

The shock-layer thickness was measured on shadowgraphs, such as shown in figure 2(a), and stagnation-point location was determined from photographs of stream patterns, such as that shown in figure 2(b). These measurements were used in developing the present correlation method for predicting shock envelopes. Additional experimental results, previously unpublished, were used to check the validity of the method for bodies of different geometry and other test conditions than those of the present investigation.

The measurement utilized to define the shock shape was the shock-layer thickness, Δ, in the direction of the body axis of symmetry as a function of radial location, r, and azimuthal location, Φ, on the body. These dimensions along with parameters that define the model geometry are indicated in figure 3. Measurements made in the vertical plane of symmetry are presented in figure 4 in the normalized form Δ/d as a function of r/r_{max}.

Shock-layer thicknesses in Φ planes other than the vertical plane of symmetry were deduced from orthogonal sets of shadowgraphs taken at each angle of attack. These thicknesses were most conveniently determined at the location $r = r_t$; hence, measurements were restricted to this location. The procedure was as follows: Since both of the orthogonal views contain the most forward point of the shock, the vertical position of the plane containing the horizontal projection of the shock trace was measured from the vertical plane shadowgraph. Thus, locations of points on the shock were established in planes other than the vertical plane of symmetry. The distance Δ and the associated angle Φ corresponding to the point r_t were determined from each set of orthogonal shadowgraphs and are summarized in figure 5. The foregoing method of extracting data gives no control in the selection of the Φ plane which depends primarily on the angle of attack. No functional relationship between Δ and Φ independent of α should be interpreted from figure 5.

The line or point of convergence of the stream patterns, such as shown in figure 2(b), was interpreted as indicating the stagnation-point location. The stagnation-point locations, r_{st}, are plotted in figure 6 in the normalized form r_{st}/r_{max} as a function of angle of attack.

ANALYSIS

Shock-Layer Thickness

The method for estimating shock-layer thickness consists first of determining the thickness at zero angle of attack and then adding an increment due to angle of attack. The method is restricted to the portion of the shock contained within a cylindrical boundary whose radius is that of the vehicle, r_{max}, and is coaxial with the vehicle axis of symmetry. Charts for determining the shock layer are presented. The angle-of-attack limits of the method and an auxiliary procedure for determining the shock in the vicinity of a rounded, windward corner at large angles of attack are also given.

Shock layer at zero angle of attack.- The shock surface at zero angle of attack is determined, with minor modifications, by the method of reference 1. This method is strictly applicable to blunt bodies with sharp corners but may be extended in certain cases to bodies with rounded corners. The flow up to the sonic point on a body should be identical for both sharp- and round-cornered bodies having the same radius, R_b, if the sonic point does not lie on the rounded corner. Under this condition, the method developed in reference 1 can be considered applicable up to the sonic point for a body with round corners. If the corner radius is small, the flow on the body is nearly sonic at the point of tangency of the corner arc and the forebody arc. The method of reference 1 may then be applied to the body considered as effectively sharp cornered of radius $r_t = R_b \sin \epsilon_t$.

The shock radius R_{bs} and the center-line standoff distance Δ_o fully specify the shock at zero angle of attack. When normalized in the form R_{bs}/r_t and Δ_o/r_t, they can be expressed as functions of the body bluntness factor ϵ_t and the normal-shock density ratio ρ_2/ρ_1. These functional relationships are shown in figure 7.

Shock-layer change due to angle of attack.- A means of correlating the change in shock-layer thickness with angle of attack is suggested by a consideration of the characteristics of the data in figure 4. These characteristics are as follows: (1) The shock-layer thickness is nearly constant at the vehicle center line ($r/r_{max} = 0$) in the angle-of-attack range 0° to 50°. (2) The shock-layer thickness decreases in the direction of increasing r when $\Phi = 0^\circ$ and increases when $\Phi = 180^\circ$ with some regular function of angle of attack. It was found that the change in shock-layer thickness, $(\Delta/d)_\alpha - (\Delta/d)_o$, divided by $\sin \alpha$ and by $\cos \Phi$ (to account for sign change), resulted in a correlation function dependent on r/r_{max}; that is,

$$\eta\left(\frac{r}{r_{max}}\right) = -\frac{(\Delta/d)_\alpha - (\Delta/d)_o}{\cos \Phi \sin \alpha} \tag{1}$$

The data of figure 4 applied to equation (1) and plotted in figure 8 as a function of r/r_{max} results in good correlation up to 45° angle of attack. Correlation of data above 45° deteriorates and is omitted.

An analytical means of determining the correlation function η is desirable so that effects of shock density ratios higher than those for the present experimental data and variation in body geometry can be taken into account without additional experiment. The following analytical method is based on the premise that since the function η is valid for a large range in angle of attack, it must be valid for vanishingly small angles of attack. It was further found that the first two terms of an odd power series in r/r_{max} were sufficient to give an accurate approximation of the change in shock-layer thickness indicated experimentally in figure 4. Thus,

$$\eta\left(\frac{r}{r_{max}}\right) = -\frac{(\Delta/d)_\alpha - (\Delta/d)_o}{\cos \Phi \sin \alpha} = c_1\left(\frac{r}{r_{max}}\right) + c_3\left(\frac{r}{r_{max}}\right)^3 \tag{2}$$

For vanishingly small α the following results

$$\left[\frac{d(\Delta/d)}{d\alpha}\right]_{\alpha=0^o} = -\left[c_1\left(\frac{r}{r_{max}}\right) + c_3\left(\frac{r}{r_{max}}\right)^3\right]\cos\Phi \qquad (3)$$

The values of c_1 and c_3 required in equation (3) are determined from the equations derived in the appendix and are presented in figure 9. Estimated values for η for the present test conditions are plotted in figure 8.

Shock in vicinity of a round corner.- At large angles of attack, it is necessary to modify the predicted shock in the vicinity of a round windward corner. It should be noted in this connection that the shock standoff distance Δ considered here is measured with reference to the surface extension of the forebody radius R_b. Thus, as indicated in sketch (a), Δ does not extend to the actual vehicle surface at values of $r > r_t$. At angles of attack for which the standoff distance Δ becomes small with respect to the corner radius R_c, the following special procedure is used to define the "corner" shock.

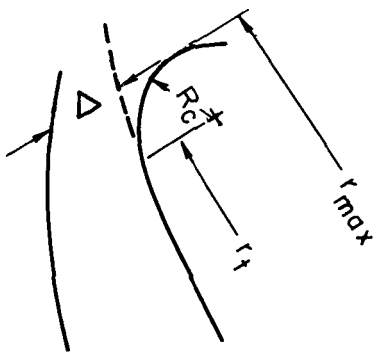

Sketch (a)

At large angles of attack, the stagnation point is in the vicinity of the round corner, and it is assumed that the flow is locally two-dimensional. Accordingly, a two-dimensional shock is patched tangentially to the basic shock in such a manner that mass-flow continuity is preserved. The procedure used is a simple geometrical construction illustrated in the sketch of figure 10 and is based on unique angular properties of a two-dimensional shock solution obtained from correlation of numerical results of reference 3. The assumption is made, as in reference 1, that the shock inclination, θ_s^*, and the normalized shock-layer thickness, Δ^*/R_{cs}, depend only on the sonic-point inclination, θ_b^*, on the body at a given shock density ratio. Associated, then, with θ_b^* are two readily determined angles Λ_s and Λ_c that give, respectively, the loci of the most forward points and the centers of possible two-dimensional shocks with respect to the sonic-point location.

$$\tan\Lambda_s = \frac{R_{cs}\sin\theta_s^*}{R_{cs}(1-\cos\theta_s^*)+\Delta^*} = \frac{\sin\theta_s^*}{(1-\cos\theta_s^*)+(\Delta^*/R_{cs})}$$

$$\tan\Lambda_c = \frac{R_{cs}\sin\theta_s^*}{R_{cs}\cos\theta - \Delta^*} = \frac{\sin\theta_s^*}{\cos\theta_s^* - (\Delta^*/R_{cs})}$$

Since, in this case, there is no sharp corner to fix the sonic-point inclination, the angle for a round (cylinder) body found from reference 3 is used. (Significantly, this angle is nearly independent of shock density ratio and is in fair accord with Newtonian values.) The angles θ_b^*, θ_s^*, Λ_s, and Λ_c are presented in the chart of figure 10 as a function of shock density ratio. This chart is applied as follows: Given the shock density ratio, the sonic point is located

at the point on the body surface inclined at the appropriate angle, θ_b^*, with respect to the normal of the free-stream direction. Lines inclined at the angles Λ_s and Λ_c with respect to the free-stream direction are extended from the sonic point and directed as indicated in the sketch of figure 10. These lines subtend a family of line segments taken in the free-stream direction. One of these, when swung about its center on the line defined by Λ_c, will coincide tangentially with the basic shock. This line segment, denoted R_{cs} in the sketch, constitutes the corner shock solution.

Shock Correlation Limits

Limitation of angle of attack in $\Phi = 0^\circ$ plane.- It is required to determine the angle-of-attack limit of the correlation method for flight conditions and vehicle geometry other than those of the present tests. For a sharp-cornered vehicle, the limiting angle is readily specified and is that angle which gives shock attachment at the corner ($\Phi = 0^\circ$ and $r/r_{max} = 1$). This results when the change in shock thickness at the corner as given by equation (2) is numerically equal to the shock thickness at the corner when $\alpha = 0^\circ$. This condition is expressed by

$$\alpha_{max} = \sin^{-1} \frac{[\Delta^*/d]}{c_1 + c_3} \tag{4}$$

In some instances it will be found that the bracketed term in equation (4) is larger than unity. Shock attachment will not then be predicted by the correlation function. The maximum angle of attack for such cases is conservatively chosen as that angle for which the shock inclination at $r/r_{max} = 1$ and $\Phi = 0^\circ$ is normal to the free-stream direction. For calculative purposes the inclination of the shock trace is expressed in the most simple terms with respect to a plane normal to the body axis of symmetry. The shock inclination is determined as follows: The displacement, x, of the shock trace from the plane located at Δ_o from the body at the center line is

$$x = R_{bs}\left[1 - \cos\left(\sin^{-1}\frac{r}{R_{bs}}\right)\right]_{\alpha=0^\circ} + d\left[c_1\left(\frac{r}{r_{max}}\right) + c_3\left(\frac{r}{r_{max}}\right)^3\right]\cos\Phi\sin\alpha \tag{5a}$$

The derivative of (5a) with respect to r gives the slope of the shock

$$\frac{dx}{dr} = \tan\left(\sin^{-1}\frac{r}{R_{bs}}\right)_{\alpha=0^\circ} + \frac{d}{r_{max}}\left[c_1 + 3c_3\left(\frac{r}{r_{max}}\right)^2\right]\cos\Phi\sin\alpha \tag{5b}$$

Setting the slope given by equation (5b) equal to $\tan\alpha$ at $\Phi = 0^\circ$ and $r/r_{max} = 1$ is equivalent to placing the shock at that point normal to the free-stream direction; thus,

$$\tan \alpha_{max} = \tan\left(\sin^{-1}\frac{d}{R_{bs}}\right) + 2(c_1 + 3c_3)\sin \alpha_{max} \qquad (5c)$$

Solutions for α_{max} from equation (5c) are summarized in chart form in figure 11. The maximum angle of attack for applicability of the present method for sharp-cornered bodies is then the smaller of the angles given by equation (4) or figure 11.

For round-cornered bodies, shock attachment is precluded at all angles of attack and the maximum angle is defined if the basic shock becomes tangent to the "minimum" corner shock. The minimum corner shock is that supported by a cylinder of radius R_c for which the shock radius is $R_{cs} = R_c \sin \theta_b^*/\sin \theta_s^*$ (fig. 10).

Limitation of r/r_{max} in $\Phi > 90^\circ$ planes.- In certain cases, for $\Phi > 90^\circ$, it is necessary to limit the r/r_{max} range of validity of predicted shock traces to values less than unity. This limitation exists since the predicted shock trace, in contradiction to experiment, can have an inflection point in the interval $0 < r/r_{max} < 1$. The location of the inflection point, or where the curvature is 0, is therefore used as the limiting value for r/r_{max}. The interrelationship between r/r_{max}, Φ, and α at the inflection point is

$$\frac{r_{max}}{R_{bs}} + 12c_3\left[1 - \left(\frac{r}{r_{max}}\frac{r_{max}}{R_{bs}}\right)^2\right]^{3/2}\frac{r}{r_{max}}\cos \Phi \sin \alpha = 0 \qquad (6)$$

The left side of equation (6) is the curvature of the shock trace determined from equation (5a).

Stagnation-Point Location

The stagnation-point location, r_{st}/r_{max}, as a function of angle of attack is approximated by a curve which fits given stagnation-point locations and the derivatives of these stagnation-point locations with respect to α at $\alpha = 0^\circ$ and at some large angle of attack, α_N, to be specified. In addition, the function must increase monotonically over the angle-of-attack range. A simple function having these properties is

$$\frac{r_{st}}{r_{max}} = b_1 \sin \alpha + b_n \sin^n \alpha \qquad (7)$$

The reason for the choice of $\sin \alpha$ will become apparent in a later discussion.

The constant b_1 in equation (7) is the derivative $d(r_{st}/r_{max})/d\alpha$ at $\alpha = 0^\circ$ and is found as follows: The stagnation or body streamline at a small angle of attack is specified as entering the shock at some point on the shock inclined at a small angle $d\theta_s$ with respect to a plane normal to the free-stream

direction as shown in sketch (b). The point on the shock is chosen so that the stagnation streamline behind the shock is deflected in a direction normal to the

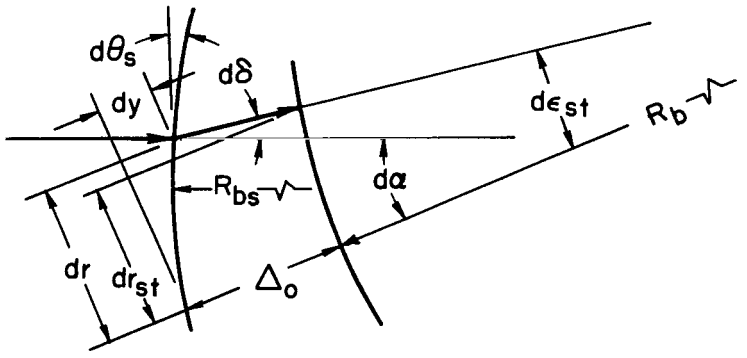

Sketch (b)

body surface. The stagnation stream in the shock layer is assumed to be a straight line since one can show that for small deflections, $d\delta$, the curvature of the stream behind the shock is vanishingly small (of the order $d\delta/R_{bs}$). It is to be noted at this point that the above properties of the stagnation streamline differ from those used in reference 2. It was assumed in reference 2 that the streamline enters the shock at the point where the shock surface is normal to the free-stream direction. The displacement of the stagnation streamline from the normal point of an asymmetric shock (angle of attack) assumed herein was adopted on the basis of the findings of reference 4. The following, from oblique shock relationships and from inspection of sketch (b), may then be written:

$$d\alpha - d\epsilon_{st} = d\delta = \left(\frac{\rho_2}{\rho_1} - 1\right) d\theta_s$$

$$dr = (R_b + \Delta_o) d\epsilon_{st}$$

$$dr_{st} = dr - \Delta_o(d\alpha - d\delta)$$

and, at dr, from equation (5b) $d\theta_s \rightarrow dx/dr$ as $\alpha \rightarrow d\alpha$; thus,

$$d\theta_s = \frac{dr}{R_{bs}} + 2c_1\, d\alpha$$

Omitting the algebraic details involved, one may combine the above relationships to give

$$\frac{d\left(\frac{r_{st}}{r_{max}}\right)}{d\alpha} = b_1 = \frac{\left(\frac{R_{bs}}{r_{max}}\right)\left[1 + \left(\frac{\rho_2}{\rho_1} - 1\right)(1 - 2c_1)\right]}{\left(\frac{\rho_2}{\rho_1} - 1\right) + \left(\frac{R_{bs}}{R_b}\right)\left[1 + \left(\frac{\rho_2}{\rho_1} - 1\right)\frac{\Delta_o}{R_{bs}}\right]} \tag{8}$$

In order to determine b_n and n required in equation (7), the stagnation-point location and its variation with angle of attack must be specified at some large angle α_N. At this large angle the flow is assumed to be two-dimensional at the windward corner. The geometry of the corner has an important bearing on the behavior of the stagnation point. Two corner geometries will be considered: a sharp corner and a rounded corner.

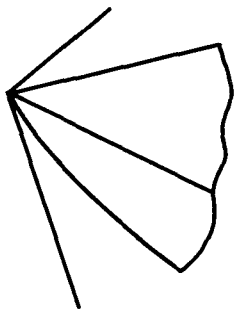

For a sharp corner (sketch (c)), the stagnation point will coincide on the corner, $r_{st}/r_{max} = 1$ and the derivative $d(r_{st}/r_{max})/d\alpha = 0$ when either two-dimensional shock attachment occurs[1]

$$\alpha_N \approx 90^\circ + \epsilon_t - \sin^{-1}\left(\frac{\frac{\rho_2}{\rho_1} - 1}{\frac{\rho_2}{\rho_1} + 1}\right) \tag{9a}$$

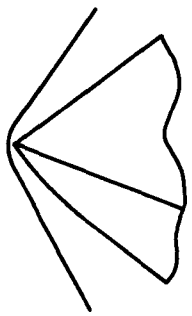

Sketch (c)

or the afterbody and forebody inclinations are numerically equal thus presenting a symmetric wedge element with respect to the free-stream direction

$$\alpha_N = 45^\circ + \frac{\epsilon_\alpha + \epsilon_t}{2} \tag{9b}$$

The smaller of the angles given by equations (9) is chosen for α_N. The angle α_N, provided $r_{st}/r_{max} = 1$ and $d(r_{st}/r_{max})/d\alpha = 0$, along with b_1 given by equation (8) allows equation (7) to be solved for n and b_n for sharp-cornered vehicles.

$$n = \frac{b_1 \sin \alpha_N}{b_1 \sin \alpha_N - 1} \tag{10}$$

$$b_n = \frac{-b_1}{n \sin^{n-1} \alpha_N} \tag{11}$$

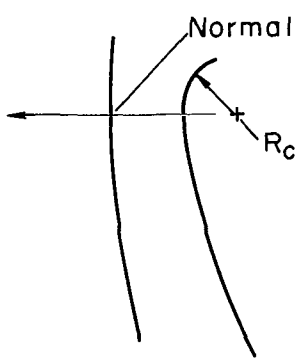

Sketch (d)

In the case of a round corner an additional consideration is made. It is assumed that the Newtonian stagnation (most forward) point is valid when a streamwise line from this point passes normally through the corner shock as indicated in sketch (d). The angle of attack, when this condition exists, is found among the graphical solutions for the corner shock previously discussed with reference to

[1]The term $\sin^{-1}\{[(\rho_2/\rho_1) - 1]/[\rho_2/\rho_1) + 1]\}$ is the maximum wedge angle for attached two-dimensional flow for an ideal gas in the limiting case $M = \infty$ but gives a good approximation for Mach numbers down to $M = 3$ in air. Its application to real gas flow is assumed.

figure 10 and, again, is that angle for which the corner shock radius has the particular value $R_{cs} = R_c \sin \theta_b^*/\sin \theta_s^*$. The smallest among these graphically determined angles, that given by equation (9b), or that found from figure 11, is chosen for α_N. It is further assumed that the derivative of the stagnation point with respect to angle of attack as well as its location is correctly given by Newtonian theory at α_N and for $\alpha > \alpha_N$. The Newtonian values for the stagnation-point location and its derivative with respect to angle of attack at $\alpha = \alpha_N$ are

$$\frac{r_{st}}{r_{max}} = \frac{r_t}{r_{max}} + \frac{R_c}{r_{max}} (\sin \alpha_N - \sin \epsilon_t) \tag{12}$$

and

$$\frac{d(r_{st}/r_{max})}{d\alpha} = \frac{R_c}{r_{max}} \cos \alpha_N \tag{13}$$

The constant b_1 given by equation (8) along with the appropriate α_N and equations (12) and (13) is used in equation (7) to solve for n and b_n for round-cornered vehicles:

$$n = \frac{(b_1 - R_c/r_{max})\sin \alpha_N}{(b_1 - R_c/r_{max})\sin \alpha_N - (r_t/r_{max} - R_c \sin \epsilon_t/r_{max})} \tag{14}$$

$$b_n = \frac{R_c/r_{max} - b_1}{n \sin^{n-1} \alpha_N} \tag{15}$$

NUMERICAL EXAMPLES

Numerical examples are now given for calculating the shock-layer thickness at a given point on a vehicle and for calculating the stagnation-point location at a given angle of attack. The vehicle is sharp cornered, with a radius $r_t = r_{max} = (1/2)R_b$, and with $\epsilon_a = 20^\circ$ (fig. 3). The angle of attack is 30° and flight occurs at an altitude and velocity resulting in the normal-shock density ratio of $\rho_2/\rho_1 = 10$.

Shock-Layer Thickness

It is required to find the shock-layer thickness at $r/r_t = 0.8$ in the $\Phi = 45^\circ$ plane. A preliminary calculation is made to establish the angle-of-attack limit of the method as specified by equation (4) or the chart of

figure 11. The sonic-point shock-layer thickness, Δ^* at $\alpha = 0^\circ$, required in equation (4) is found by means of the geometrical relationship of reference 1 expressed as equation (16):

$$\Delta = \Delta_o + R_b(1 - \cos \theta_b) - R_{bs}(1 - \cos \theta_s) \tag{16}$$

For $\Delta = \Delta^*$, the angles θ_b and θ_s have the values corresponding to the body sonic-point location r_t

$$\theta_b = \theta_b^* = \epsilon_t = \sin^{-1} \frac{r_t}{R_b} = \sin^{-1} \frac{1}{2} = 30^\circ$$

Figures 7(a) and 7(b) are now consulted and give $R_s/r_t = 2.30$ and $\Delta_o/r_t = 0.150$ at $\epsilon_t = 30^\circ$ with $\rho_2/\rho_1 = 10$. The shock inclination corresponding to r_t may now be calculated and is

$$\theta_s = \theta_s^* = \sin^{-1} \frac{r_t}{R_{bs}} = \sin^{-1} \left(\frac{1}{2.30} = 0.435 \right) = 25.8^\circ$$

Equation (16) is evaluated for $\Delta = \Delta^*$:

$$\Delta^* = 0.150r_t + 2r_t(1 - \cos 30^\circ) - 2.30r_t(1 - \cos 25.8^\circ) = 0.188r_t$$

and, with $d/r_t = 2$; $\Delta^*/d = 0.094$. Values of c_1 and c_3, also required in equation (4), are found from figures 9(a) and 9(b) at $\epsilon_t = 30^\circ$ with $\rho_2/\rho_1 = 10$, giving

$$c_1 = 0.0275$$

$$c_3 \left(\frac{R_b}{d} \sin \epsilon_t \right)^2 = c_3(0.25) = 0.0068$$

or

$$c_3 = 0.0272$$

Equation (4) gives

$$\alpha_{max} = \sin^{-1}[0.094/(0.0275 + 0.0272) > 1]$$

which cannot be satisfied, indicating that shock attachment is not predicted by the method. The chart of figure 11 is then consulted at abscissa $\tan[\sin^{-1}(d/2R_{bs})] = \tan 25.8^\circ = 0.484$ and ordinate $2(c_1 + 3c_3) = 0.2182$ giving $\alpha_{max} \approx 30^\circ$. Since figure 11 gives conservative values, the angle of attack (30°) of the present example is not too large and calculations may proceed.

First, it is required to calculate the shock-layer thickness, Δ, at $r/r_t = 0.8$ when $\alpha = 0^\circ$. Equation (16) is again utilized but with the body and shock angles now corresponding to the body location $r/r_t = 0.8$. These angles are

$$\theta_b = \sin^{-1}\left(\frac{r}{R_b} = \frac{0.8r_t}{R_b} = 0.8 \times 0.5 = 0.4\right) = 23.6^\circ$$

$$\theta_s = \sin^{-1}\left(\frac{r}{R_{bs}} = \frac{0.8r_t}{R_{bs}} = \frac{0.8}{2.30} = 0.348\right) = 20.4^\circ$$

Equation (16) is evaluated for Δ:

$$\Delta = 0.150 + 2r_t(1 - \cos 23.6^\circ) - 2.30r_t(1 - \cos 20.4^\circ) = 0.173r_t$$

and, with $d/r_t = 2$; $(\Delta/d)_o = 0.0865$.

Finally, the shock-layer thickness $(\Delta/d)_\alpha$ at $r/r_t = r/r_{max} = 0.8$ and $\Phi = 45^\circ$ is evaluated with equation (2) written in the form

$$(\Delta/d)_\alpha = (\Delta/d)_o - [c_1(r/r_{max}) + c_3(r/r_{max})^3]\cos\Phi \sin\alpha \qquad (2)$$

Substituting the appropriate numerical values already at hand in the above equation results in the required solution

$$(\Delta/d)_\alpha = 0.0865 - [0.0275 \times 0.8 + 0.0272\times(0.8)^3]0.707 \times 0.574 = 0.072$$

Stagnation-Point Location

It is required to find the stagnation-point location at $\alpha = 30^\circ$ as given by equation (7),

$$\frac{r_{st}}{r_t} = \frac{r_{st}}{r_{max}} = b_1 \sin\alpha + b_n \sin^n\alpha \qquad (7)$$

First, the constant b_1 given by equation (8) is computed

$$b_1 = \frac{\left(\frac{R_{bs}}{r_{max}}\right)\left[1 + \left(\frac{\rho_2}{\rho_1} - 1\right)(1 - 2c_1)\right]}{\left(\frac{\rho_2}{\rho_1} - 1\right) + \left(\frac{R_{bs}}{R_b}\right)\left[1 + \left(\frac{\rho_2}{\rho_1} - 1\right)\frac{\Delta_o}{R_{bs}}\right]} \qquad (8)$$

For this purpose the following numerical values of the parameters are needed:

$$R_{bs}/R_b = (R_{bs}/r_t)(r_t/R_b) = 2.30 \times 0.50 = 1.15$$

$$\Delta_o/R_{bs} = (\Delta_o/r_t)(R_{bs}/r_t) = 0.150/2.30 = 0.0652$$

$$c_1 = 0.0275$$

$$\rho_2/\rho_1 = 10$$

Substituting the above numerical values into equation (8) results in

$$b_1 = \frac{2.30[1 + (10 - 1)(1 - 0.055)]}{(10 - 1) + 1.15[1 + (10 - 1)0.0652]} = 2.02$$

Next, the values for

$$n = \frac{b_1 \sin \alpha_N}{b_1 \sin \alpha_N - 1} \tag{10}$$

and

$$b_n = \frac{-b_1}{n \sin^{n-1} \alpha_N} \tag{11}$$

applying to a sharp-cornered vehicle are computed. The appropriate value of α_N for this computation is given as the smaller of the values given by equations (9a) and (9b)

$$\alpha_N \approx 90^\circ + \epsilon_t - \sin^{-1} \frac{(\rho_2/\rho_1) - 1}{(\rho_2/\rho_1) + 1} = 90^\circ + 30^\circ - \sin^{-1} \frac{9}{11} = 65.2^\circ \tag{9a}$$

or

$$\alpha_N = 45^\circ + \frac{\epsilon_t + \epsilon_a}{2} = 45^\circ + \frac{30^\circ + 20^\circ}{2} = 70^\circ \tag{9b}$$

Equations (10) and (11) are evaluated with $\alpha_N = 65.2^\circ$

$$n = 2.02 \times 0.908/(2.02 \times 0.908 - 1) = 1.834/0.834 = 2.20$$

$$b_n = -2.02/2.20 \times (0.908)^{1.20} = -2.02/2.20 \times 0.891 = -1.030$$

Finally, equation (7) can be evaluated to determine the stagnation-point location at $\alpha = 30^{\circ}$

$$r_{st}/r_{max} = 2.02 \times 0.500 - 1.030 \times (0.500)^{2.20} = 0.786$$

COMPARISON OF ESTIMATED AND MEASURED RESULTS

The validity of the estimated results will be assessed through comparison with measured values for the model of the present tests in the Mach number range 3.28 to 5.45. Additional comparisons between estimated and measured results are made for round-cornered bodies at Mach numbers 3.3 and 20 (in helium, see ref. 5) and for sharp-cornered bodies at Mach numbers 3.3 and 5.45.

Shock-Layer Thickness

Shock layer at zero angle of attack.- A comparison of estimated and measured shock traces for blunt vehicles at zero angle of attack is shown in figure 12. The upper two cases involve a vehicle with a small corner radius. In these cases it was assumed that the flow was sonic at the point of tangency, r_t, of the corner and forebody radius. The good agreement of estimated and measured shock traces indicates the usefulness of this assumption. The remaining cases are bodies with sharp corners. Good agreement between estimated and measured shock shapes again results. The foregoing estimates were made using charts 7(a) and 7(b) based on the method of reference 1.

Shock-layer thickness at angle of attack.- First, comparisons are made of estimated and measured shock-layer thicknesses at angle of attack in the vertical plane of symmetry. Next, comparisons are made of estimated and measured shock-layer thickness changes at angle of attack in planes other than the vertical plane of symmetry.

The shock-layer thickness estimated by adding the effect of angle of attack to the shock-layer thickness at zero angle is compared with measured values in figure 13. Good agreement results for the configurations shown. It should be noted that among the improvements of the present correlation method over that of references 1 and 2 is that it extends the estimation of the shock layer to angles of attack other than zero for flat-faced bodies. In one case shown, the angle of attack is within the range of the method of reference 2. The values estimated by the method of reference 2 and by the present method are in fair accord with each other and with measured values.

Comparisons are made between estimated and measured changes in shock-layer thickness due to angle of attack at a fixed radial location ($r = r_t$) in figure 14. For this comparison the data of figure 5 were correlated by means of

equation (1) and were plotted as a function of Φ. The estimated values indicated were calculated with equation (3a). Good agreement between estimated and measured values is shown for each Mach number of the tests.

Stagnation-Point Location

The experimental and predicted stagnation-point locations as found in the present investigation for the test model at Mach number 3.28 (in air) are plotted as a function of angle of attack in figure 6. Good agreement is shown. Also plotted are experimental results as found for a similar model tested in helium at Mach number 20. The shock density ratios involved in both air and helium test results are approximately 4. Agreement between the data and with estimated values substantiates the predicted result that the shock and stagnation-point locations depend primarily on the normal shock density ratio appropriate to the flight conditions and are relatively insensitive to the isentropic exponent of the gases involved.

A comparison between experimental and predicted results of the stagnation-point location for a sharp-cornered vehicle at Mach number 3.3 is made in figure 15. The agreement is satisfactory for both the present method and that of reference 2. The method of reference 2, however, is limited to the angle-of-attack range up to $\alpha = \epsilon_t = 30^\circ$ for this case. At this angle of attack, the value for the stagnation point predicted by the method of reference 2 is not in as good agreement with experiment as is that given by the present method.

Predicted stagnation-point locations at shock density ratios of 16 and infinity (Newtonian flow) are also indicated in figure 15. Experimental results are not available for assessing the accuracy of predicted stagnation-point locations at large normal shock density ratios. However, some confidence in the present method for predicting stagnation-point locations at large shock density ratios may be based on the fact that the results converge toward Newtonian values with increasing shock density ratio. It is to be noted from figure 15 that a significant error in the stagnation point results if the assumption is made that the experimental values obtained at typical wind-tunnel flow shock density ratios (4 to 6) adequately represent results that would be attained at shock density ratios (16) involved in atmospheric entry.

CONCLUDING REMARKS

A method was developed with which shock envelopes and stagnation-point locations can be predicted for blunt bodies at angle of attack. The method is based on a simple function which correlates the effect of angle of attack and body geometry on shock-layer thickness. The method is applicable to perfect gas flows and to equilibrium flow of real gases. The effects of atmospheric constituents and altitude enter solely through the normal shock density ratio appropriate to the flight velocity.

Predicted shock envelopes were compared with experimental values for air flows in the Mach number range 3.28 to 5.45 and the angle-of-attack range up to 50°. Satisfactory agreement between predicted and experimental shock envelopes and stagnation-point locations was found in the range of flow conditions covered by the comparisons.

Methods for predicting pressure distributions were not considered in the present investigation. At low angles of attack, $\alpha < \epsilon_t$, the method of reference 1 for sharp-cornered vehicles can be applied to give approximate pressure distribution for round-cornered vehicles, provided the corner radius is small with respect to the vehicle diameter. The effects of corner radius size and of high angle of attack on pressure distribution require further investigation.

Ames Research Center
National Aeronautics and Space Administration
Moffett Field, Calif., Sept. 18, 1963

APPENDIX A

EVALUATION OF CONSTANTS FOR EQUATION (2)

The following derivation gives the equations for c_1 and c_3 required in equation (2). For convenience, some of the notation of reference 1 as indicated in sketch (e) is initially utilized. The final results, however, are given in the present notation.

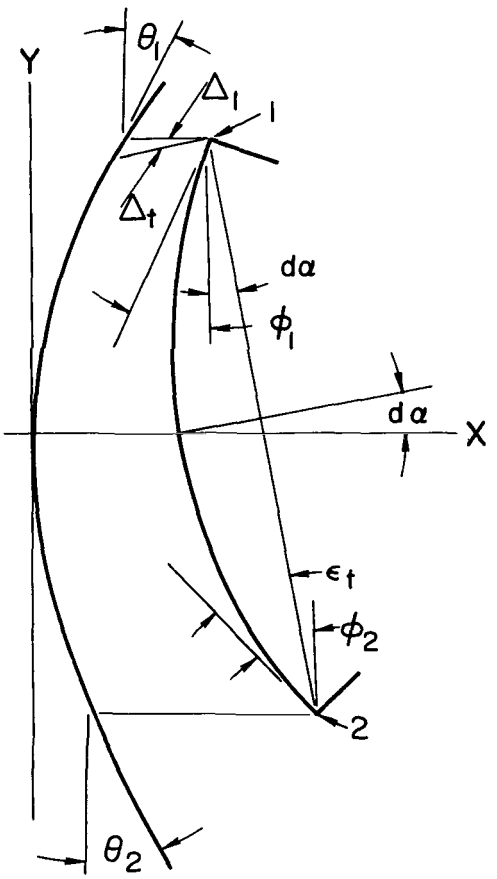

Sketch (e)

First, the change in the shock thickness Δ_t due to a small change in angle of attack from $\alpha = 0$ is determined at the sonic-point location r_t. The relationship between Δ_t in the body coordinate system used here and Δ_1 in the wind axis coordinate system of reference 1 is for small α

$$\Delta_1[\tan(\alpha + \theta_1)\sin\alpha + \cos\alpha] = \Delta_t \qquad \text{(A1)}$$

The geometric relationship among Δ_1, X_1, and Y_1 is

$$\Delta_1 = X_1\left[1 - \frac{Y_1}{X_1}\tan\left(\frac{\theta_1}{2}\right)\right] \qquad \text{(A2)}$$

where X_1 and Y_1 are given by equations (4) in reference 1. In terms of r_t, they are

$$\frac{X_1}{r_t} = \frac{2\left\{|\cos\alpha| - |\sin\alpha|\left[\dfrac{\sin\theta_2}{(\Delta/R)_2 + (1 - \cos\theta_2)}\right]\right\}}{\dfrac{\sin\theta_1}{(\Delta/R)_1 + (1 - \cos\theta_1)} + \dfrac{\sin\theta_2}{(\Delta/R)_2 + (1 - \cos\theta_2)}} \qquad \text{(A3)}$$

and

$$\frac{Y_1}{X_1} = \frac{\sin\theta_1}{(\Delta/R)_1 + (1 - \cos\theta_1)} = G_1 \text{ , etc.} \qquad \text{(A4)}$$

The values of θ, Δ/R, and, therefore, G (at a given shock density ratio) are functions of the sonic-point inclination angle φ which is related to angle of attack in the vertical plane of symmetry by

$$\varphi_1 = \epsilon_t - \alpha \quad \text{and} \quad \varphi_2 = \epsilon_t + \alpha$$

Thus, $d\alpha = -d\varphi_1 = d\varphi_2$. Choosing $d\varphi$ positive, $G_1 = G - (dG/d\varphi)d\varphi$ and $G_2 = G + (dG/d\varphi)d\varphi$. The differentiation is carried out resulting in

$$G_{1,2} = G\left(1 \mp \left\{\frac{\frac{d\theta}{d\varphi}}{\tan\theta} - G\,\frac{\left[\frac{d(\triangle/R)}{d\varphi} + \sin\theta\,\frac{d\theta}{d\varphi}\right]}{\sin\theta}\right\} d\varphi\right) \tag{A5}$$

Equations (A1) through (A4) are combined and, with $\cos\alpha = 1$ and $\sin\alpha = d\varphi$, there results

$$\left(\frac{\triangle_t}{r_t}\right)_{d\varphi} = \frac{2(1 - G_2\,d\varphi)}{G_1 + G_2}\left[1 - G_1 \tan\left(\frac{\theta_1}{2}\right)\right]\left[\tan(d\varphi + \theta_1)d\varphi + 1\right] \tag{A6}$$

The differential of equation (A6) is required and, with the relationships $\tan(\theta_1/2) = \tan(\theta/2) - (1/2)\sec^2(\theta/2)(d\theta/d\varphi)d\varphi$ and $\theta_1 = \theta - (d\theta/d\varphi)d\varphi$, is determined by expanding the right-hand term and retaining only the linear terms in $d\varphi$. Dividing the resulting differential by $d\alpha$ gives

$$\frac{d(\triangle/r_t)}{d\alpha} = \left\{\left[1 - G\tan\left(\frac{\theta}{2}\right)\right]\left(\frac{d\theta}{d\varphi} + \frac{\tan\theta}{G} - 1\right) - \frac{G\tan(\theta/2)}{\sin\theta}\,\frac{d(\triangle/R)}{d\varphi}\right\}\frac{d\varphi}{d\alpha} \tag{A7}$$

In order to evaluate (A7), the values of the derivatives $d\theta/d\varphi$ and $d(\triangle/R)/d\varphi$ are required. Equations (1), (2), and (3) of reference 1 for $\alpha = 0^\circ$ are combined to give the following relationship between θ and φ:

$$\frac{\sqrt{1 + 4\left[\frac{1 - (f/2)(\rho_s/\rho_o)}{(\rho_1/\rho_o) - 1}\right]\frac{\sin\varphi}{\sin\theta}} - 1}{2\sin\varphi} = \frac{1}{\frac{1}{2}\left(\frac{\rho_\theta}{\rho_o} - 1\right)\sin 2\theta + \frac{\rho_* V_*}{\rho_o V_o}\cos\varphi - \tan\frac{\varphi}{2} + \tan\frac{\theta}{2}} \tag{A8}$$

The derivative $d\theta/d\varphi$ is determined from equation (A8). The derivative $d(\triangle/R)/d\varphi$ can then be found with the relationship

$$\frac{\triangle}{R} = \frac{\sin\theta}{\frac{1}{2}\left(\frac{\rho_\theta}{\rho_o} - 1\right)\sin 2\theta + \frac{\rho_* V_*}{\rho_o V_o}\cos\varphi} \tag{A9}$$

given as equation (1) in reference 1. The resulting derivatives are somewhat cumbersome and are not repeated herein. With $d\theta/d\varphi$ and $d(\Delta/R)/d\varphi$ determined, values for equation (A7) giving the change in shock-layer thickness at the sonic point for small changes in angle of attack may be computed as a function of $\epsilon_t = \theta^*_{b_{\alpha=0^o}}$ for various values of the normal shock density ratio.

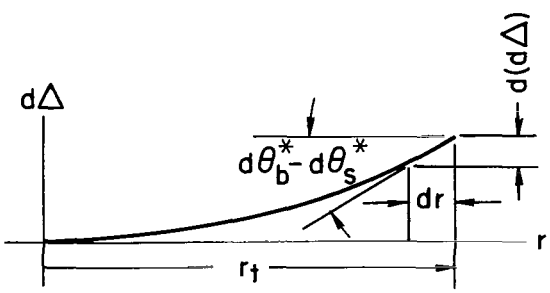

Sketch (f)

Next, the constants c required in equation (2) are determined. Sketch (f) indicates the change in shock-layer thickness as a function of r for small changes in angle of attack, $|d\alpha| = |d\theta^*_b| = |d\varphi|$. At $r = r_t$, the relative rotation of the shock trace with respect to the body is $d\theta^*_b - d\theta^*_s$ in terms of the present notation. Thus at r_t

$$d(d\Delta) = (d\theta^*_b - d\theta^*_s)dr$$

Equating the above in derivative form with the derivative of equation (2) at $r = r_t$ gives the identity

$$1 - \frac{d\theta^*_s}{d\theta^*_b} = 2\left[c_1 + 3c_3\left(\frac{r_t}{r_{max}}\right)^2\right] \tag{A10}$$

Equation (2) with $d\theta^*_b/d\alpha = 1$ (choosing positive $d\Delta$) and equation (A10) are used to solve for the constants c giving the results

$$\left.\begin{aligned} c_1 &= \frac{3\,\frac{d(\Delta/r_t)}{d\alpha} - \left(1 - \frac{d\theta^*_s}{d\theta^*_b}\right)}{4} \\ \text{and} \\ c_3 &= \frac{\left(1 - \frac{d\theta^*_s}{d\theta^*_b}\right) - \frac{d(\Delta/r_t)}{d\alpha}}{16\left(\frac{R_b \sin \epsilon_t}{d}\right)^2} \end{aligned}\right\} \tag{A11}$$

where $r_t = R_b \sin \epsilon_t$. Equations (A11) along with the shock charts of reference 2 were used to compute values for the charts of figure 9.

REFERENCES

1. Kaattari, George E.: Predicted Shock Envelopes About Two Types of Vehicles at Large Angles of Attack. NASA TN D-860, 1961.

2. Kaattari, George E.: Predicted Gas Properties in the Shock Layer Ahead of Capsule-Type Vehicles at Angle of Attack. NASA TN D-1423, 1962.

3. Fuller, Franklyn B.: Numerical Solutions for Supersonic Flow of an Ideal Gas About Blunt Two-Dimensional Bodies. NASA TN D-791, 1961.

4. Swigart, R. J.: A Theory of Asymmetric Hypersonic Blunt-Body Flows. AFOSR-TN-62-2232, 1962.

5. Marvin, Joseph G., Tendeland, Thorval, and Kussoy, Marvin: Apollo Forebody Pressure and Heat-Transfer Distributions in Helium at $M_\infty = 20$. NASA TM X-854, 1963.

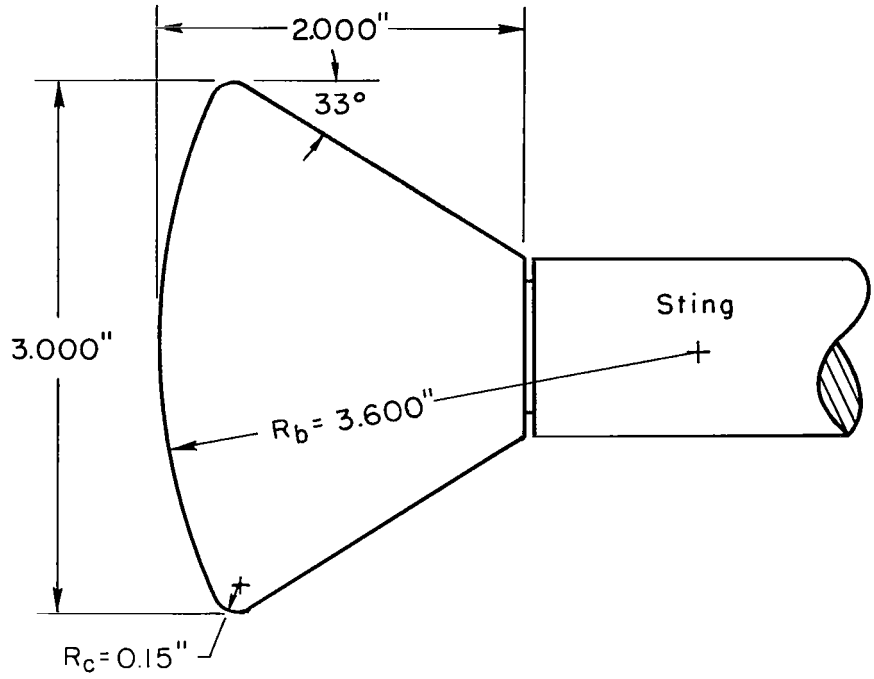

Low angle model

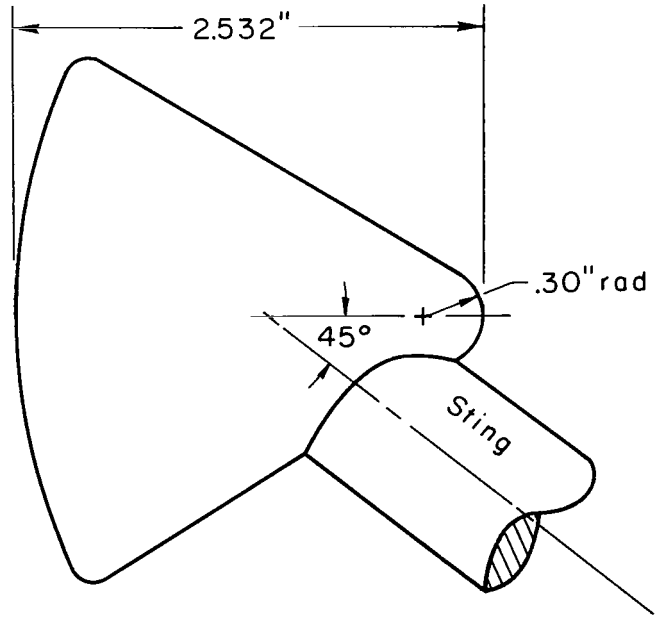

High angle model

Figure 1.- Model and support.

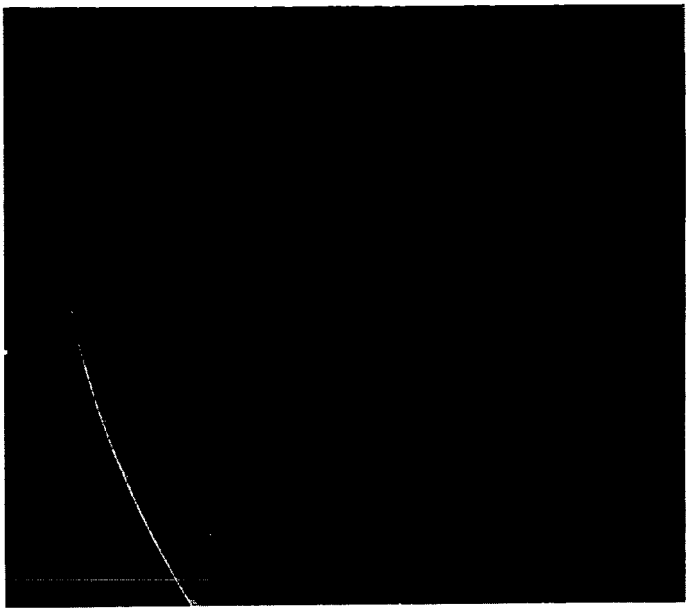

(a) Shock at $\alpha = 20^{\circ}$; M = 4.06.

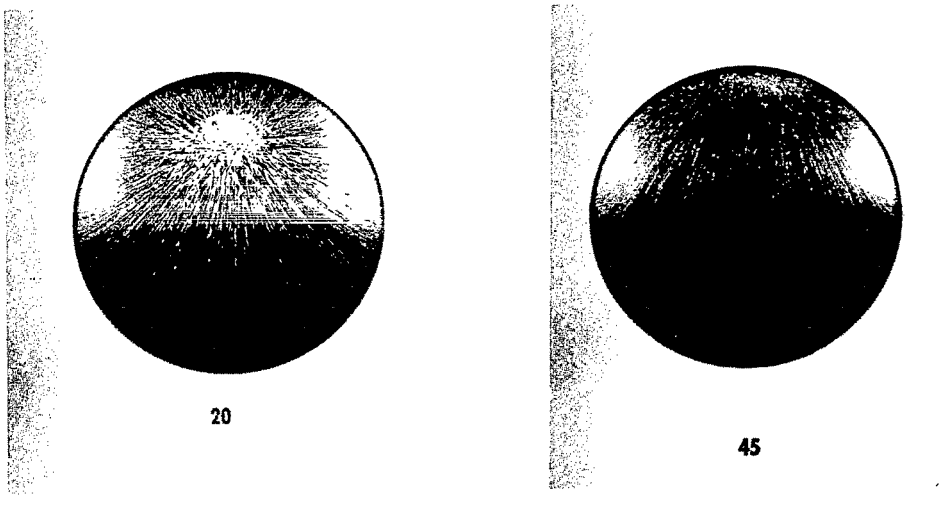

(b) Stream patterns at $\alpha = 20^{\circ}$ and 45°; M = 3.28.

Figure 2.- Typical photographs of shock and stream patterns.

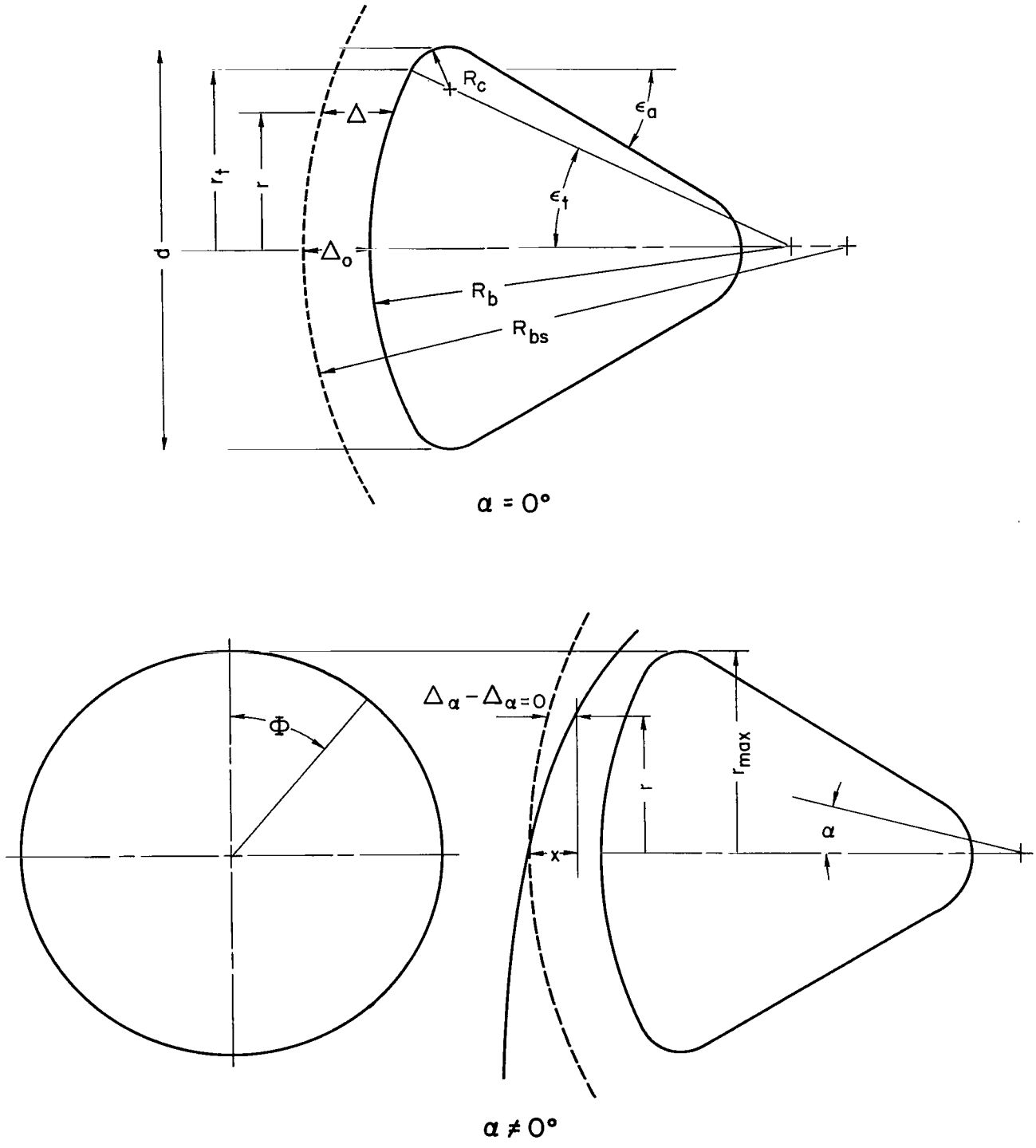

Figure 3.- Illustration of nomenclature.

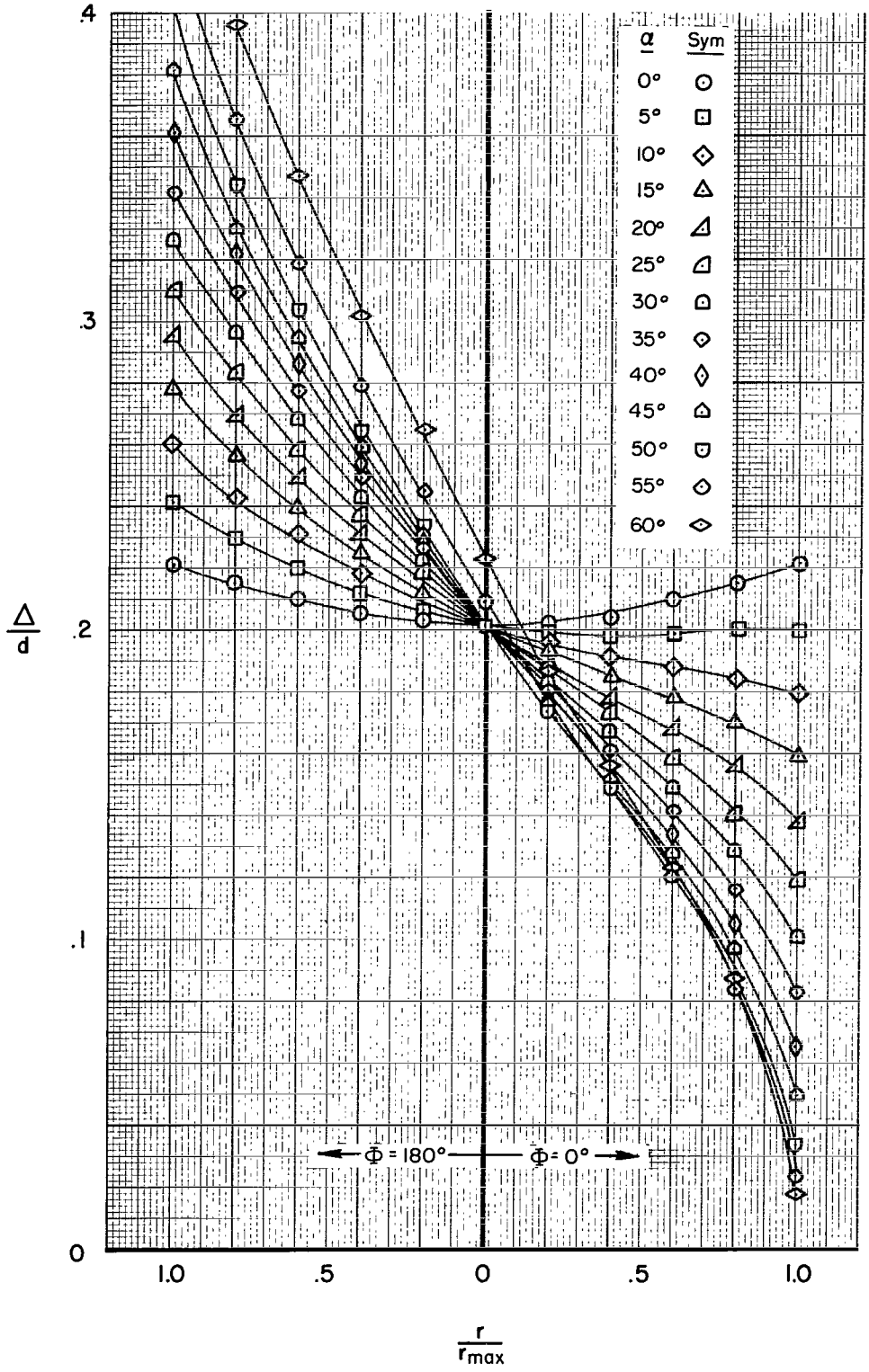

(a) M = 3.28

Figure 4.- Measured shock-layer thickness in vertical plane of symmetry.

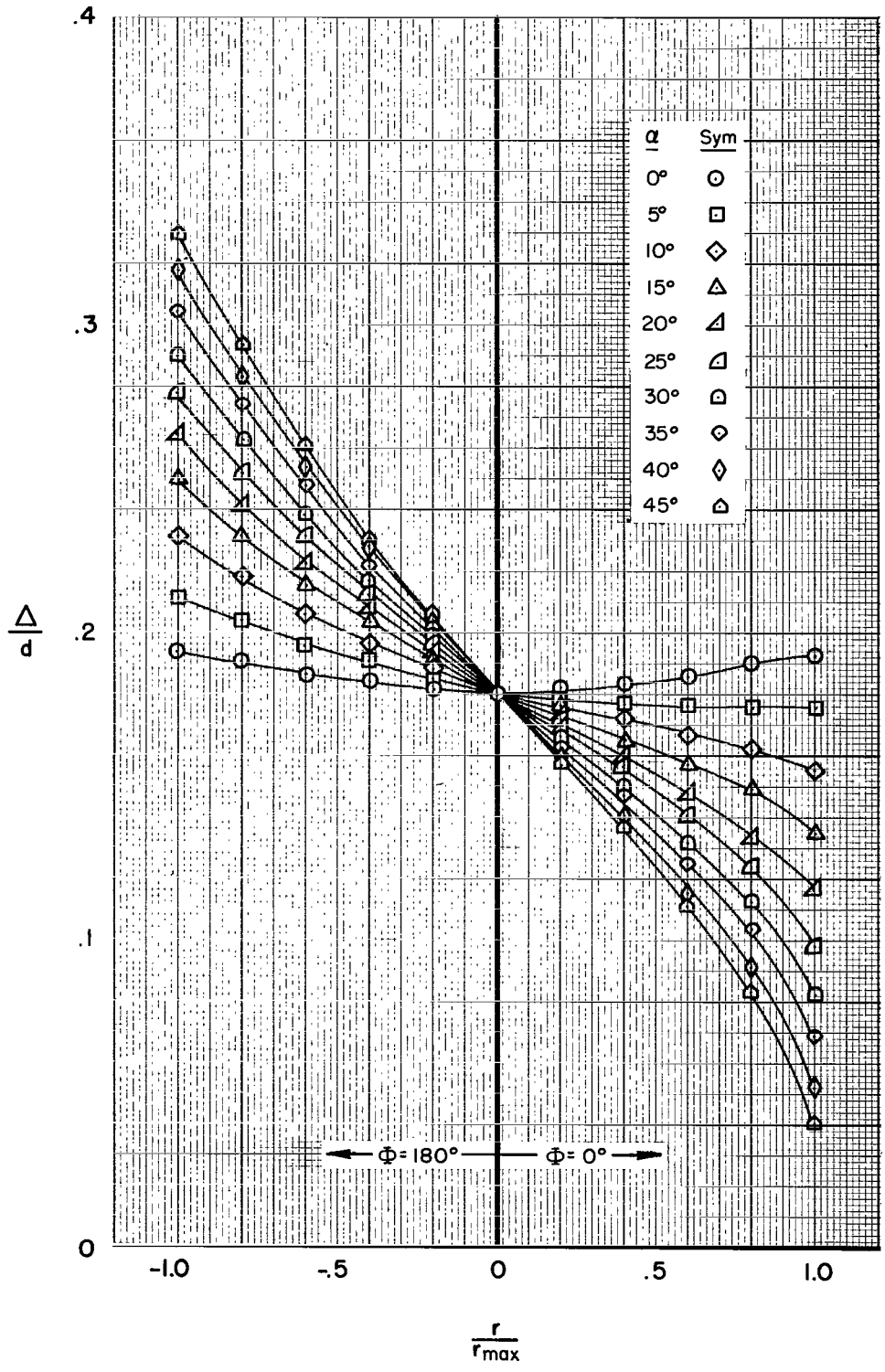

(b) M = 4.06

Figure 4.- Continued.

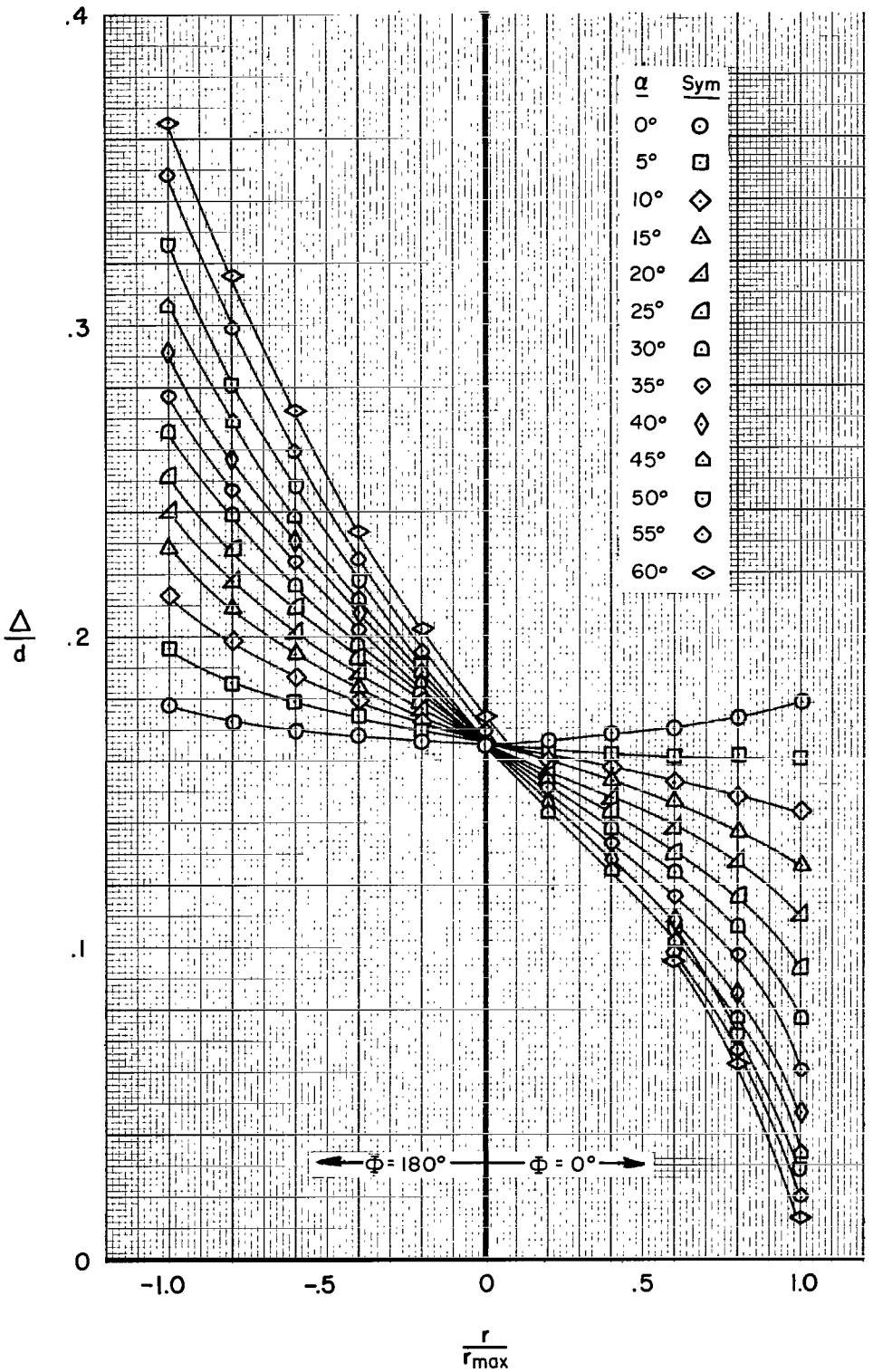

(c) M = 5.45

Figure 4.- Concluded.

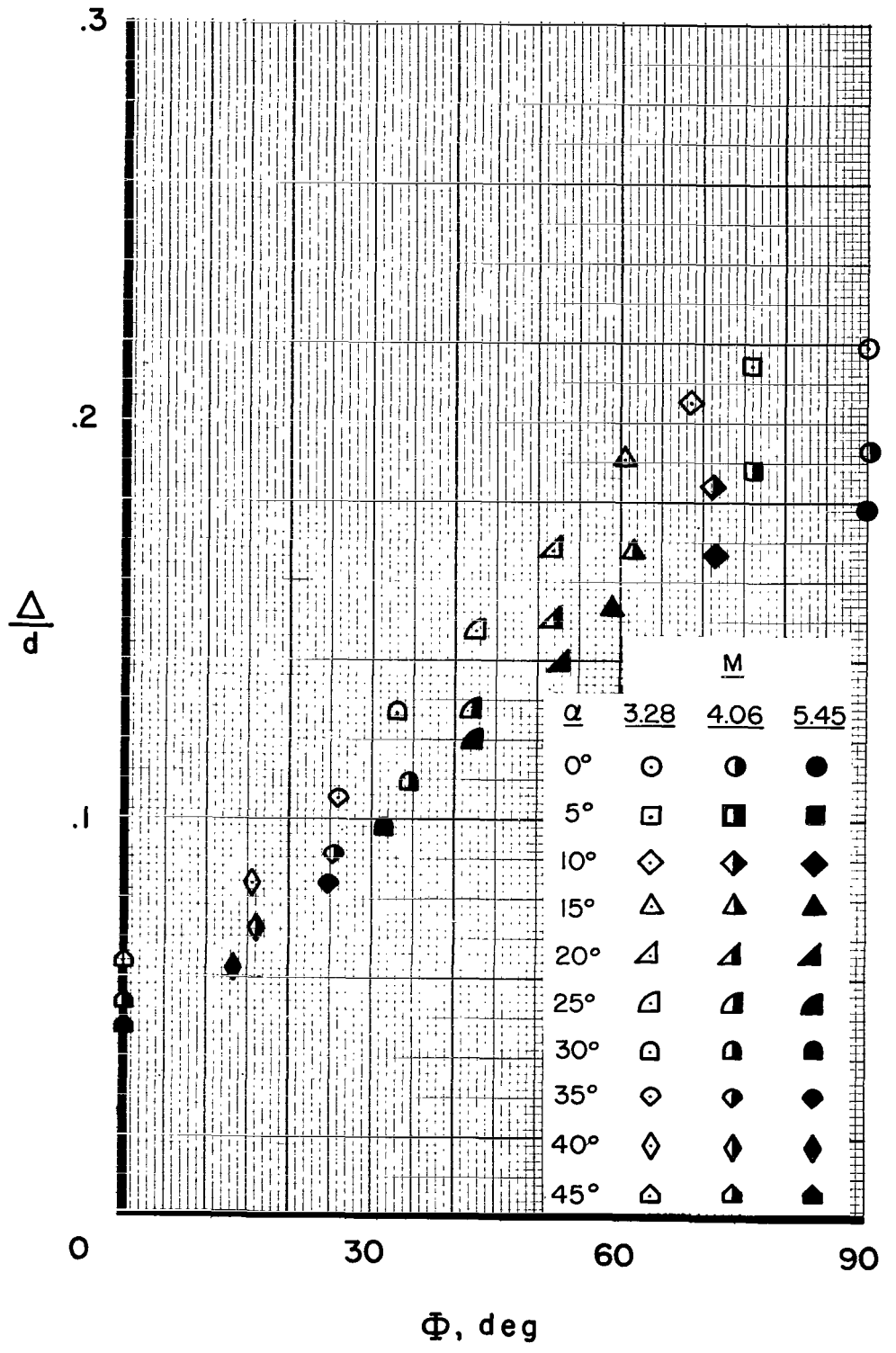

Figure 5.- Measured shock-layer thickness at $r = r_t$ in various Φ planes.

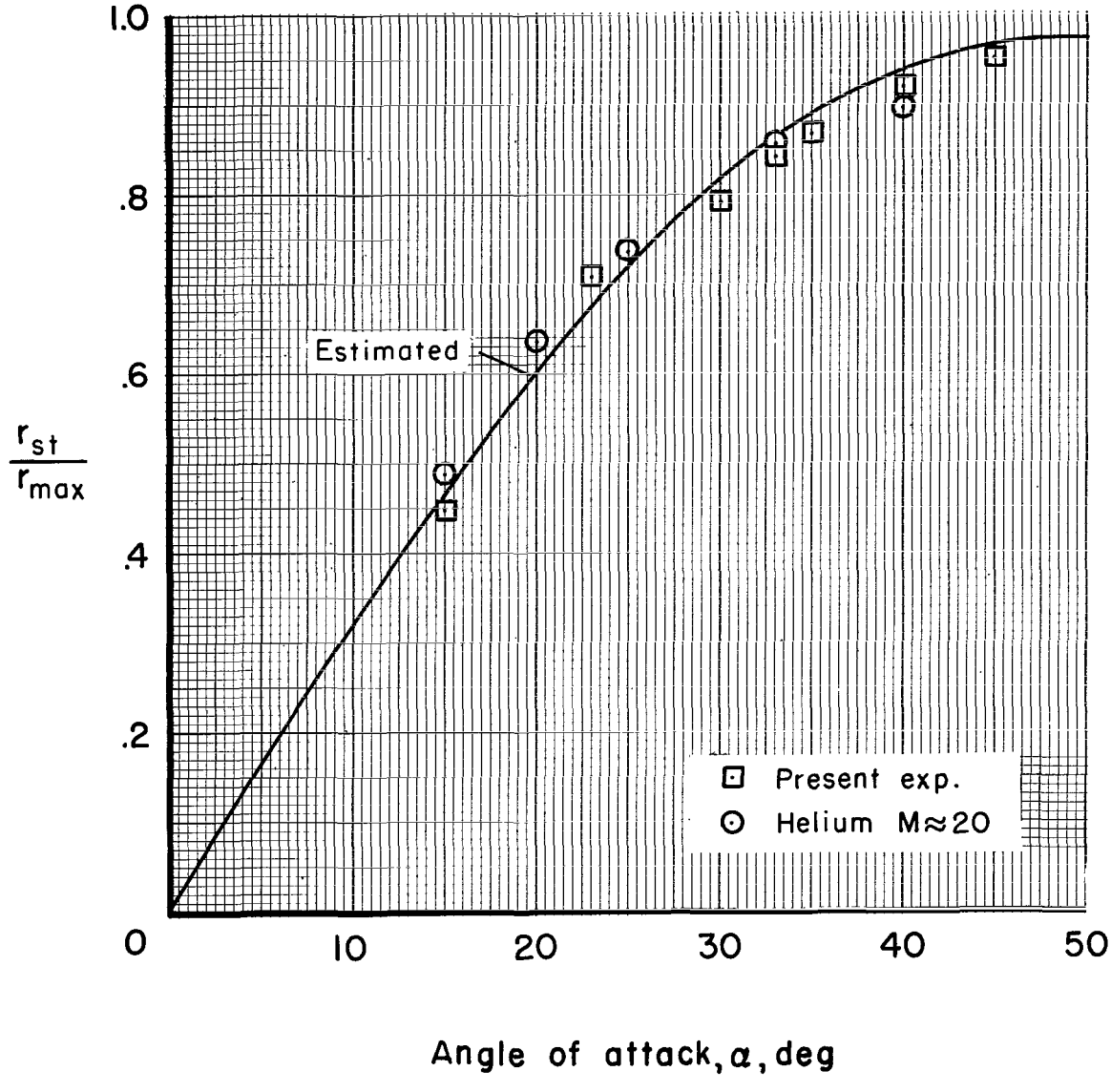

Figure 6.- Measured and estimated stagnation-point locations.

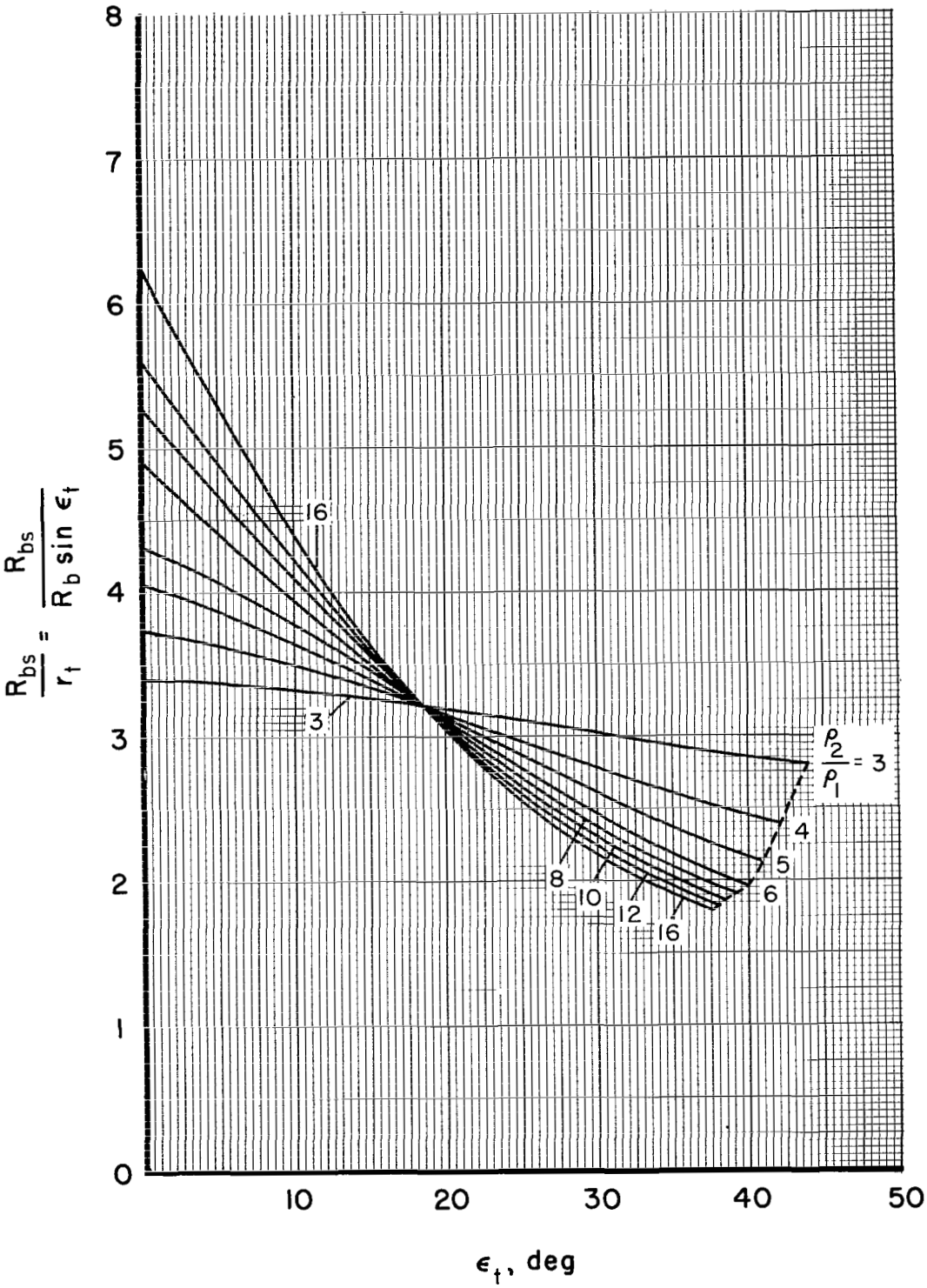

(a) Shock radius, R_{bs}.

Figure 7.- Estimated shock dimensions for $\alpha = 0^{\circ}$.

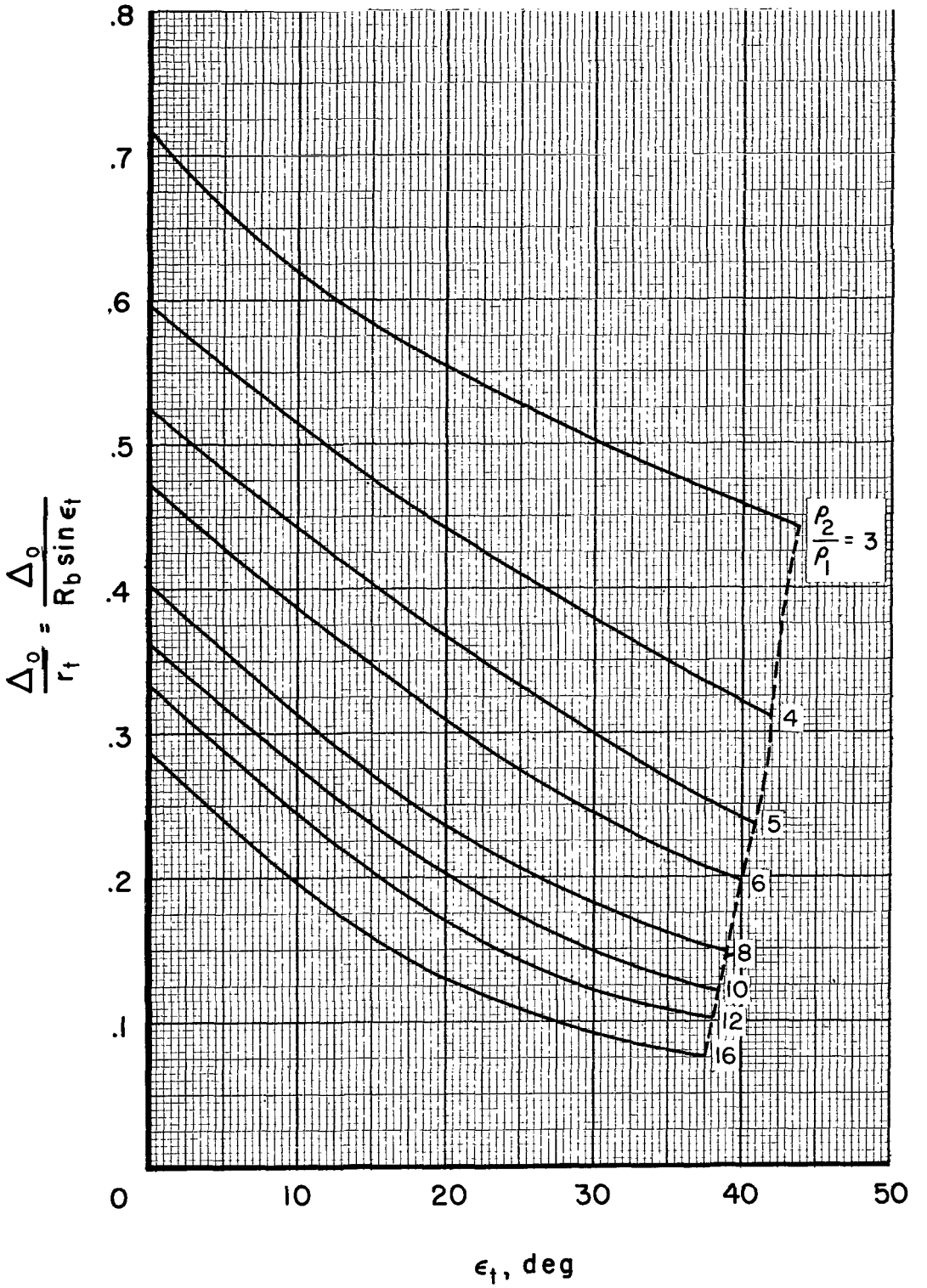

(b) Shock stand-off Δ_o.

Figure 7.- Concluded.

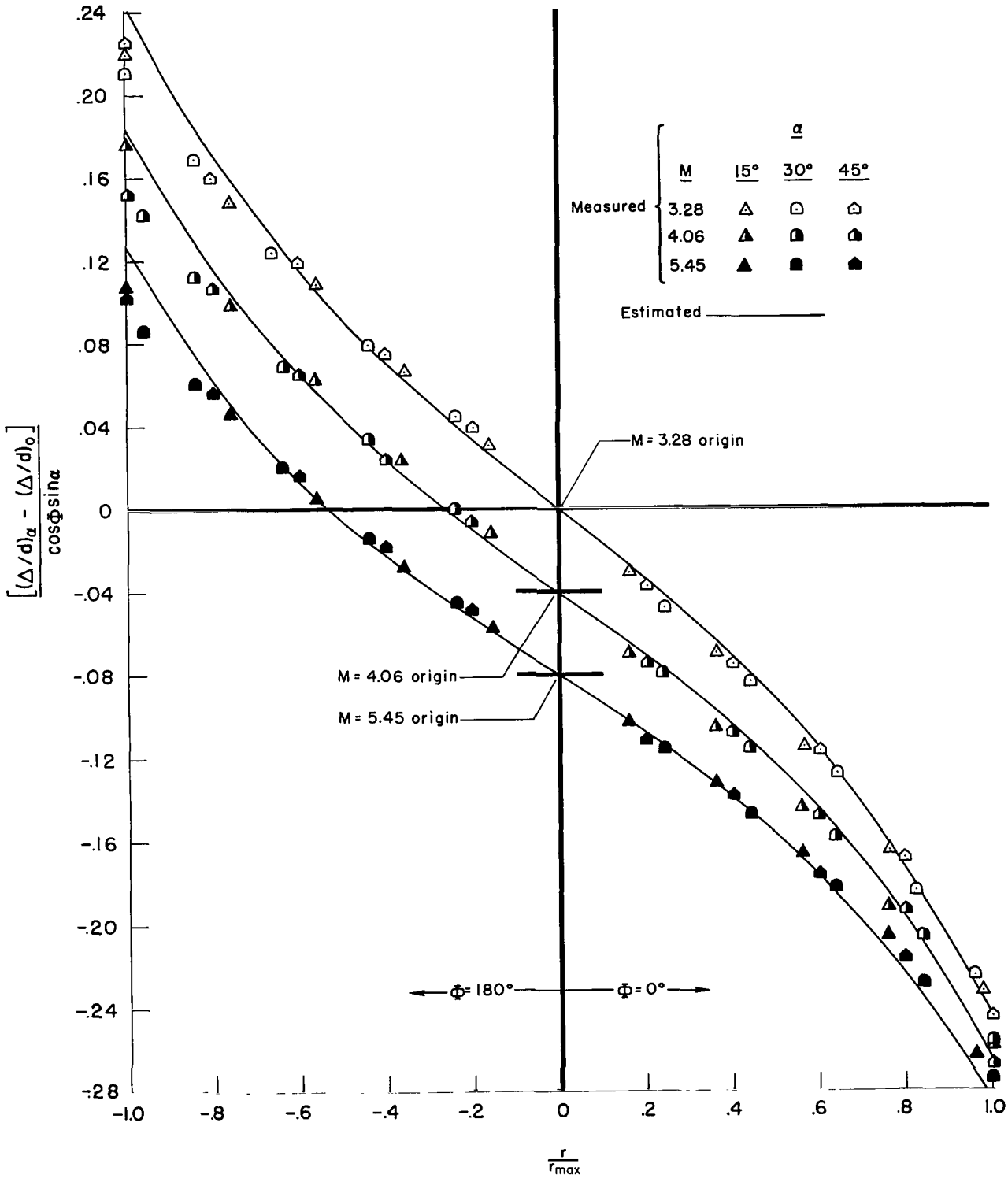

Figure 8.- Measured and estimated correlation of shock-layer thickness in vertical plane of symmetry.

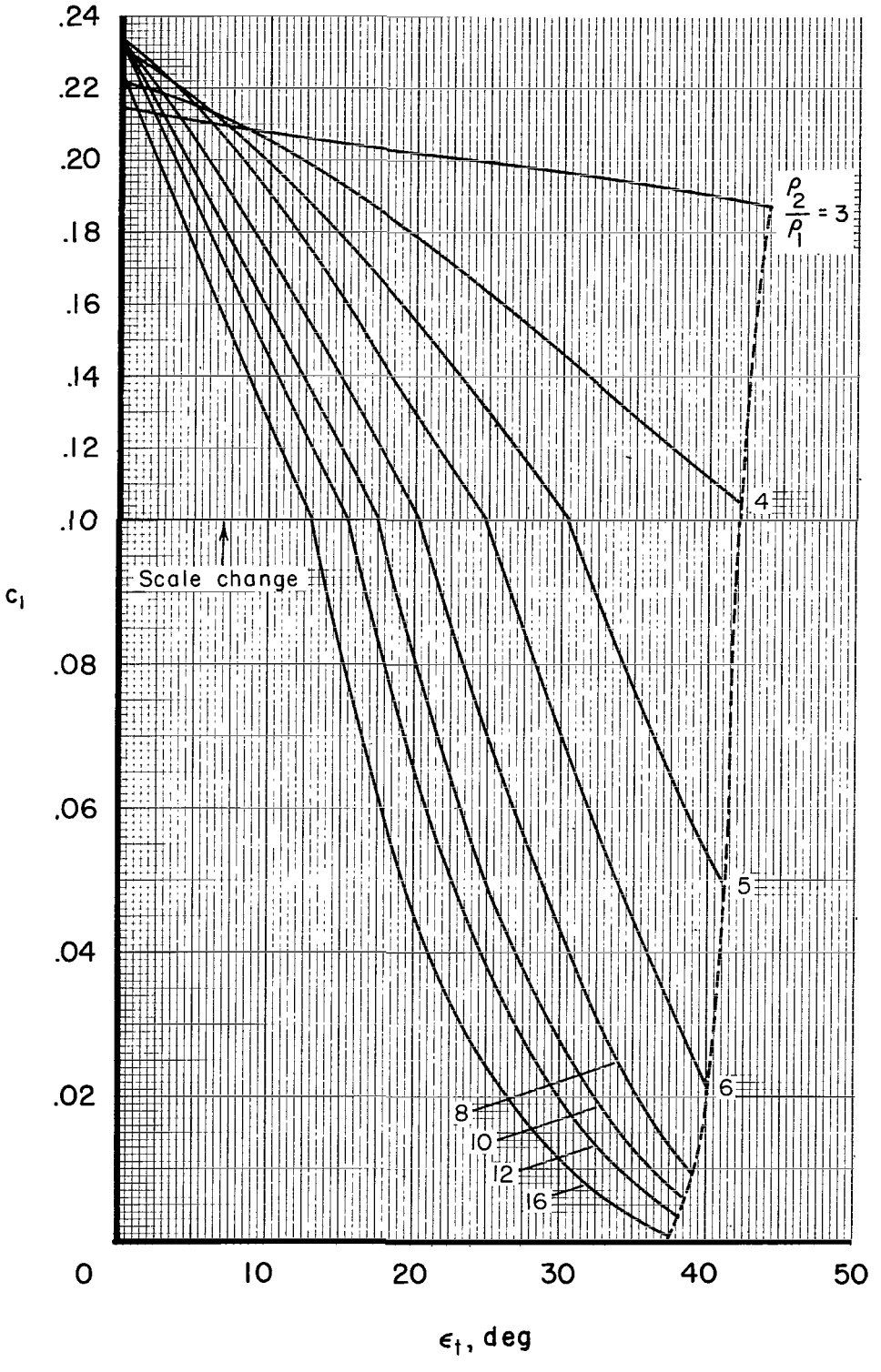

(a) Constant c_1.

Figure 9.- Estimated correlation-function constants.

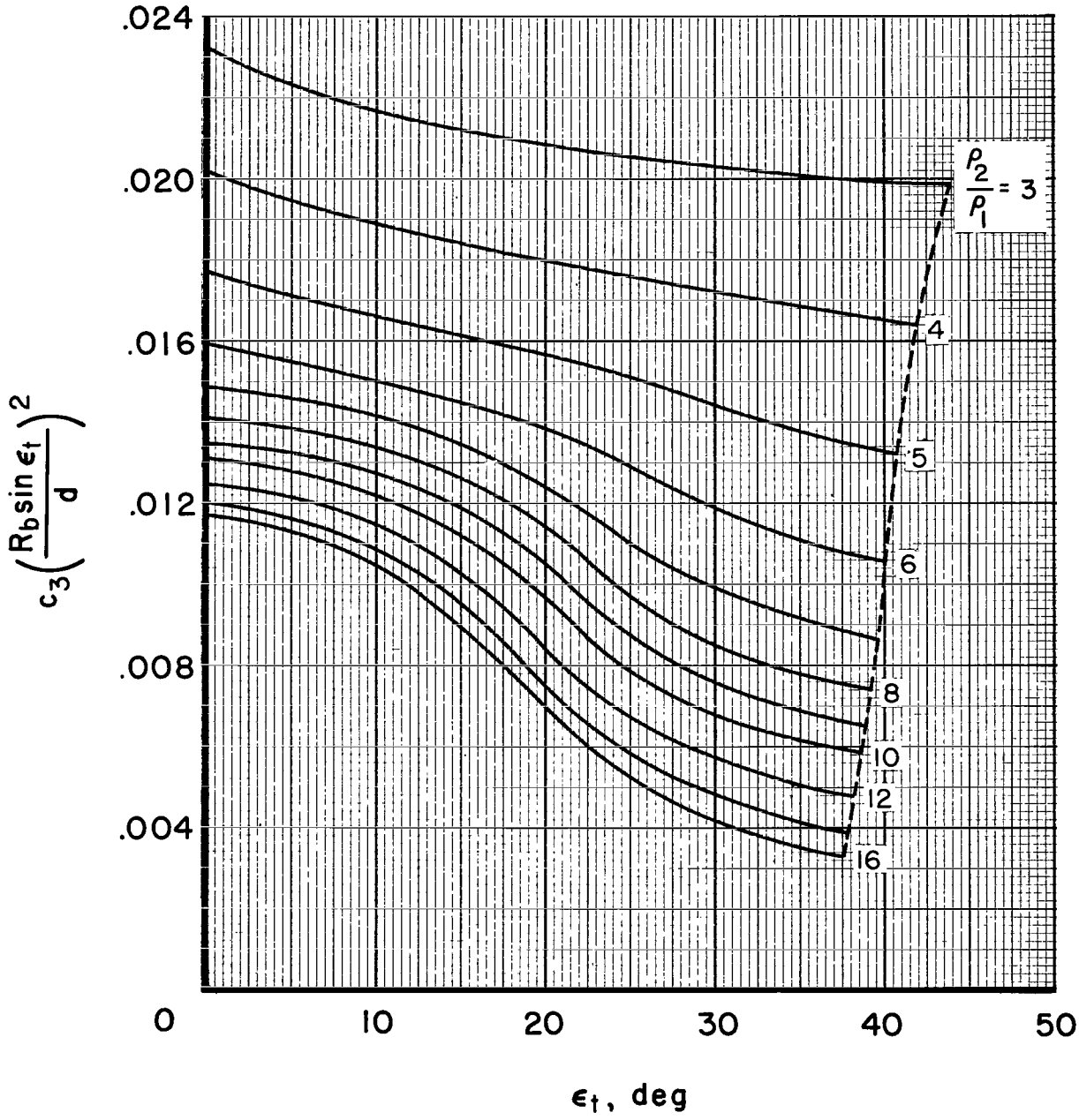

(b) Constant c_3.

Figure 9.- Concluded.

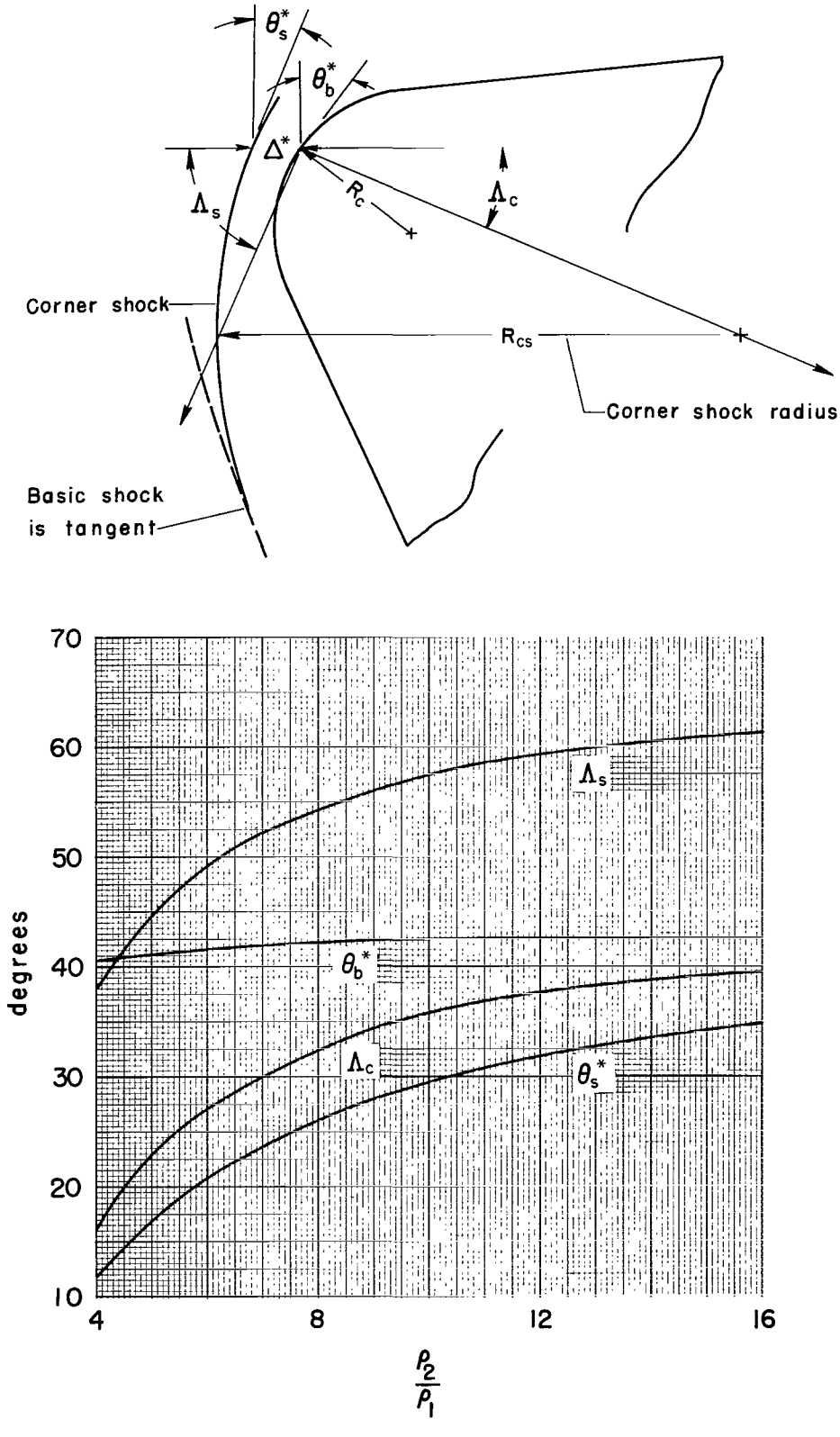

Figure 10.- Estimated extension of shock to vicinity of rounded corner.

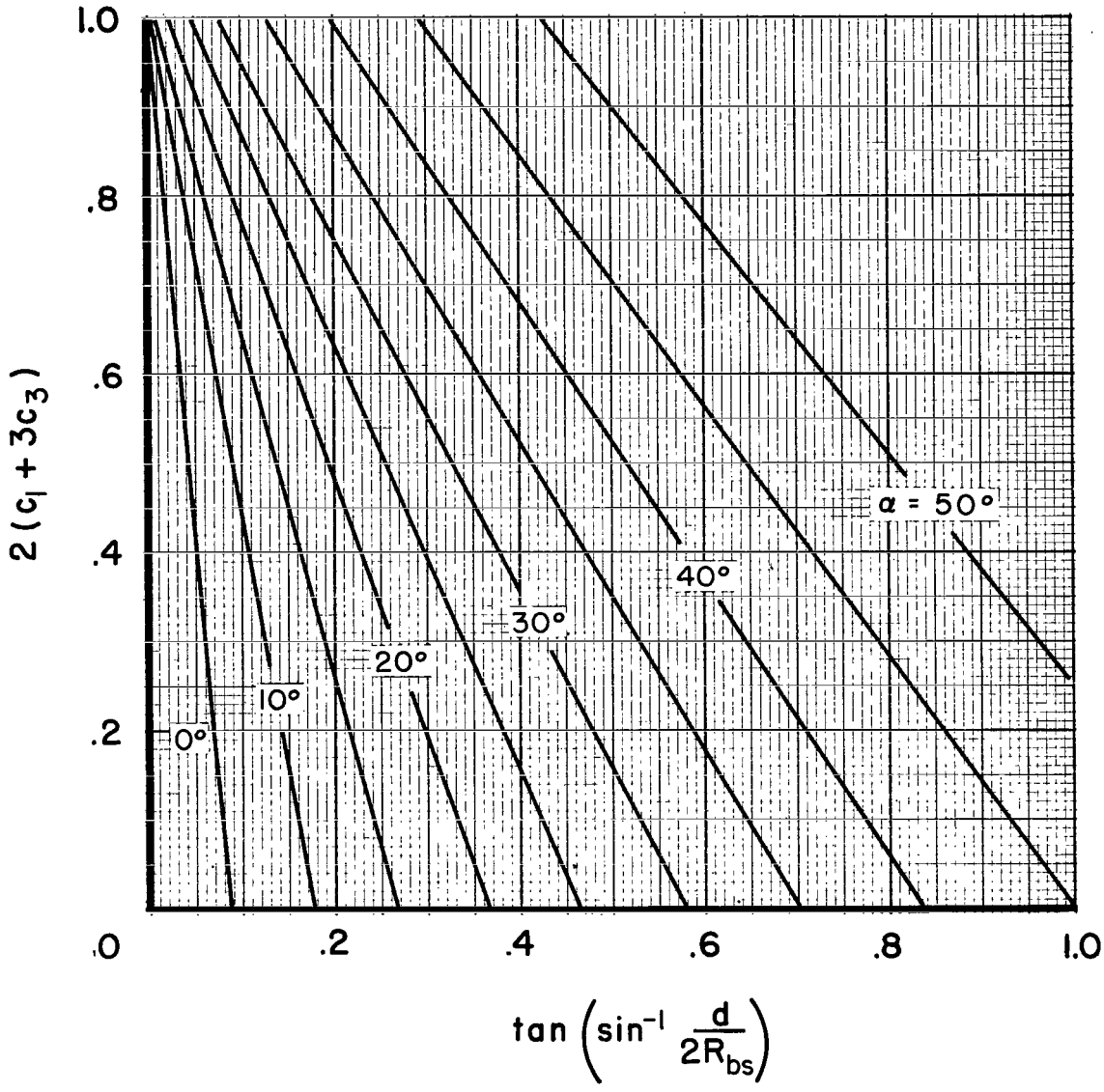

Figure 11.- Angle-of-attack limit of correlation function for sharp-cornered vehicle.

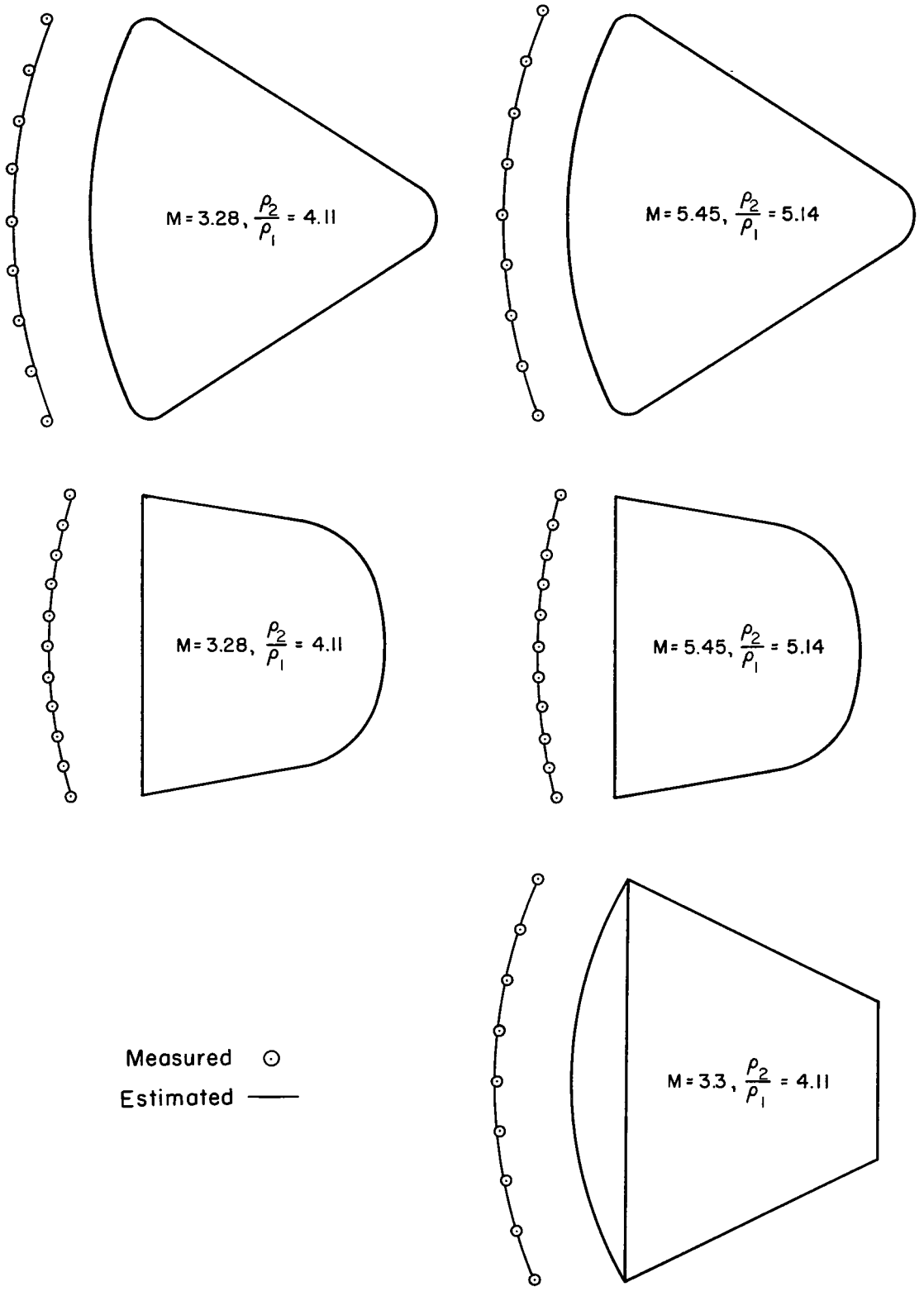

Figure 12.- Measured and estimated shock layers in vertical plane of symmetry; $\alpha = 0^{\circ}$.

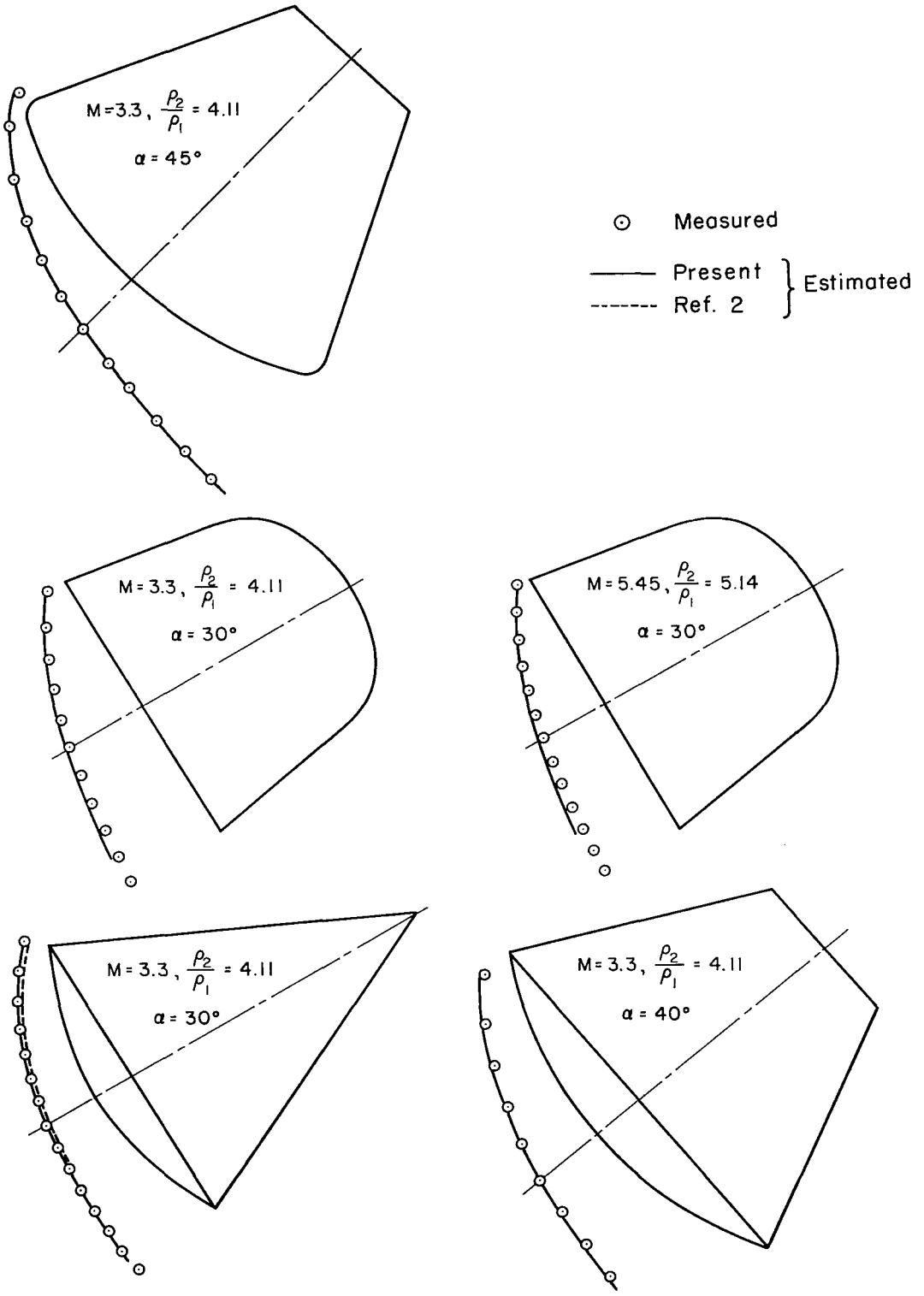

Figure 13.- Measured and estimated shock layers in vertical plane of symmetry; $\alpha \neq 0^{\circ}$.

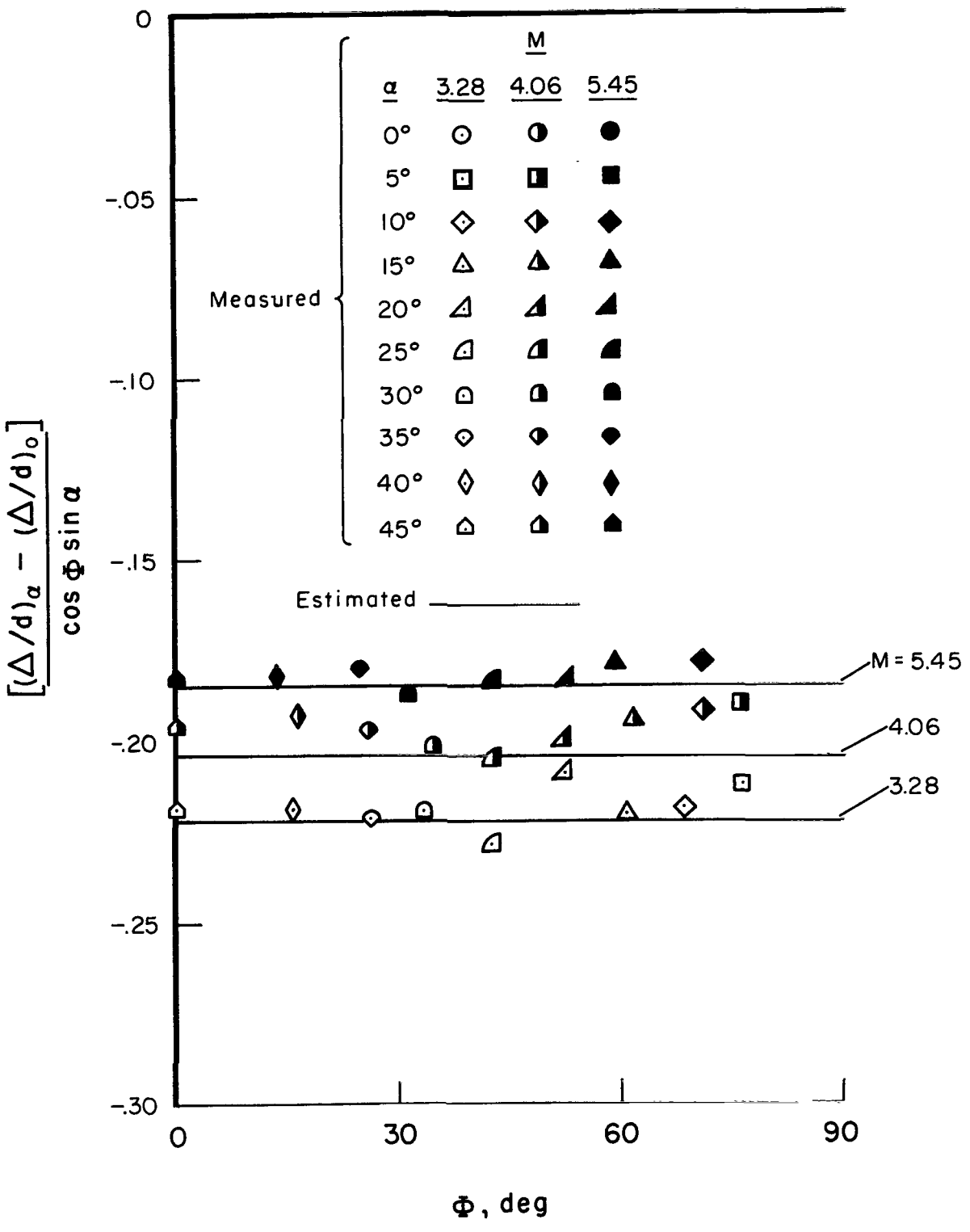

Figure 14.- Measured and estimated correlation of shock-layer thickness at $r = r_t$ in various Φ planes.

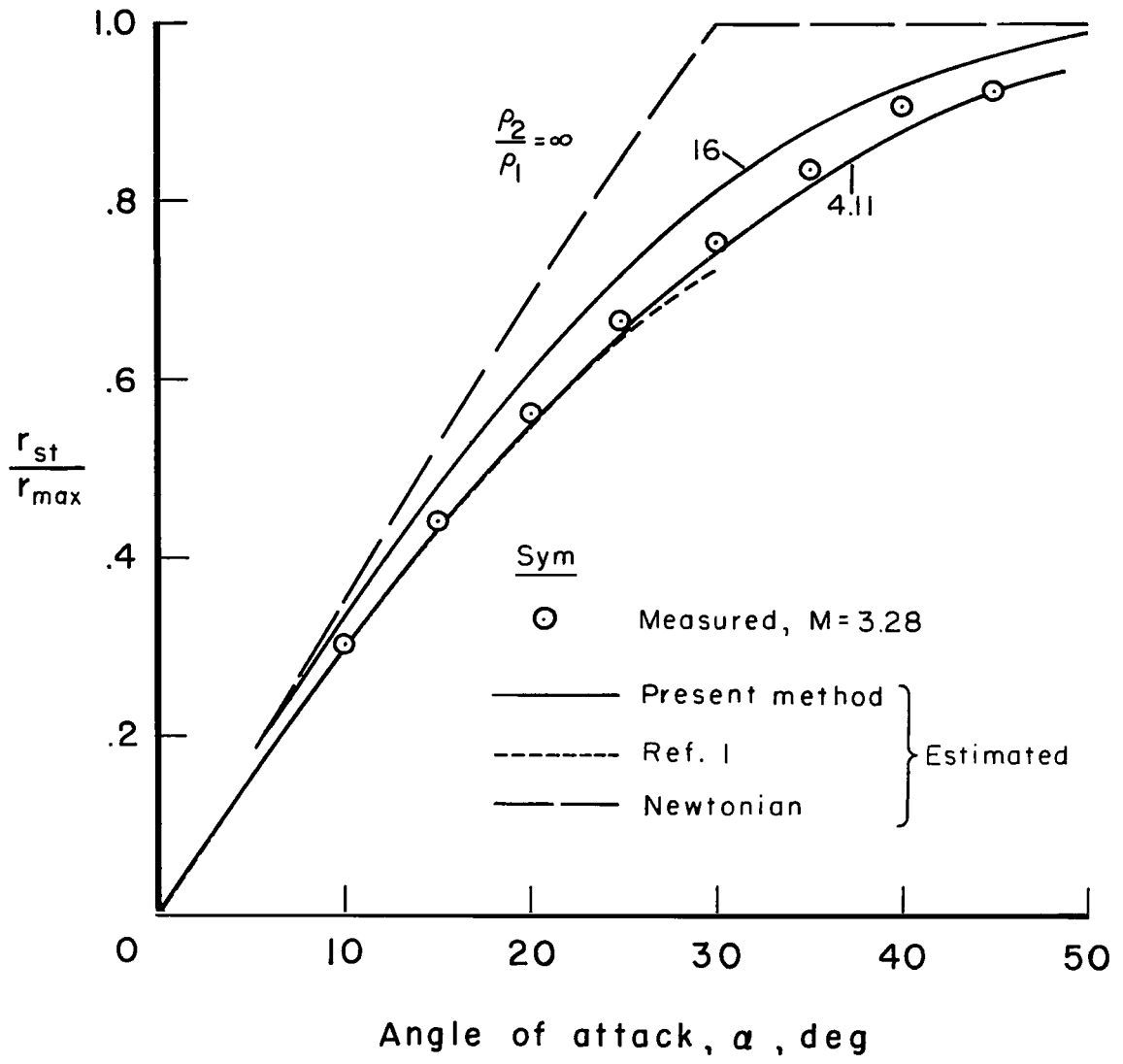

Figure 15.- Measured and estimated stagnation-point locations on sharp cornered vehicle, $\epsilon_t = 30^\circ$.